LONG-RANGE INTERNET OF THINGS: ANALYSIS OF LORA PERFORMANCE

By

Noushin Poursafar

A THESIS SUBMITTED TO MACQUARIE UNIVERSITY

FOR THE DEGREE OF MASTER OF RESEARCH

SCHOOL OF ENGINEERING

APRIL 2018

Except where acknowledged in the customary manner, the material presented in this thesis is, to the best of my knowledge, original and has not been submitted in whole or part for a degree in any university.

Noushin Poursafar

Acknowledgements

First and foremost, I would like to express my sincere gratitude to my supervisor, Professor Subhas Mukhopadhyay, who supported me throughout this project. I am also thankful to the admirable staff in the School of Engineering for their wonderful support. I wish to acknowledge Macquarie University for awarding me an international Research Training Pathway Scholarship (iRTP) and providing financial support to attend international conferences. I would like to thank ATDI Company that gave me a great chance to learn and use ICS telecom EV software and Dr. Keith Imrie who proofread the thesis and suggested some improvement to English expression. I also sincerely thank my parents, and my family as a whole, for their love and support throughout this project and my life. Last but not least, thanks to my friends for making me feel special, being there when I needed them.

List of Publications

- Noushin Poursafar, Md Eshrat E Alahi, and Subhas Mukhopadhyay, Long-range Wireless Technologies for IoT Applications: A Review, 11th International Conference on Sensing Technology (ICST), pp.310-15, 2017.
- Noushin Poursafar and Subhas Mukhopadhyay, Outdoor Coverage Area and Signal Propagation Analysis of LoRa at 915 MHz, in the final draft stage to be submitted to IEEE Trans, Instrumentation and Measurement.

Abstract

The internet of things (IoT) is a concept for a wireless network that allows objects to be sensed or controlled remotely using the internet as a carrier. The IoT is attractive for future wireless systems and it is estimated that the IoT will consist of 75 billion objects by 2025. As the IoT looks to scale up, the cellular industries are likely to use both licensed and unlicensed bands for this purpose. The Low-power Wide-Area Network (LPWAN) is one of the IoT technologies, which hires licensed and unlicensed spectrum for data transmission over long distances. Since one of the most important issues in sending and receiving data is to minimise the maintenance and deployment cost, having a knowledge of the system propagation plays a vital role in designing a reliable and cost-effective network. Therefore, the main aim of this project is to assess the propagation performance of long-range IoT technology (LoRa) as unlicensed spectrum in an LPWAN, at the frequency of 915 MHz.

To reach this goal, real-world measurements are recorded at different locations of the Macquarie University campus, Sydney, Australia. Using the measurement data, we will introduce path-loss models for Line-of-sight (LOS) and non-line-of-sight (NLOS) areas which enable operators to estimate the number of LoRa base stations required for covering a specific area.

Contents

List of Figures

List of Tables

Chapter 1
Introduction

1.1. Motivation and Objective

The Internet of Things (IoT) is a technology concept that refers to a network of smart devices that share information wirelessly without requiring human intervention. The IoT is used in different fields for various applications, such as smart buildings [1-6], smart metering [7, 8], transport logistics [9, 10], industrial monitoring [11-16], traffic safety [17-19], and environment monitoring [20]. Generally, the IoT can be categorised into two groups. Firstly, the Massive IoT that connects an enormous amount of smart devices together, such as smart metering and industrial monitoring. This category is suitable for fields that need low-cost devices with low energy consumption and a good coverage in urban areas. Secondly, Critical IoT that covers applications which need high reliability and low latency, such as traffic safety and remote-controlled surgery in healthcare.

It is forecasted that the IoT market will grow from 15.4 billion devices in 2015 to 75 billion in 2025 [21] (Figure 1.1). To reach the predicted volume, the IoT market will need an average growth rate of approximately 18%. As a result, the IoT has attracted the attention of researchers.

It is quite challenging to choose the right wireless technology for an IoT application, because there are many wireless technologies available with different features. Figure 1.2 provides information about the range and throughput of available technologies in the IoT market, and can be helpful in selecting the appropriate technology.

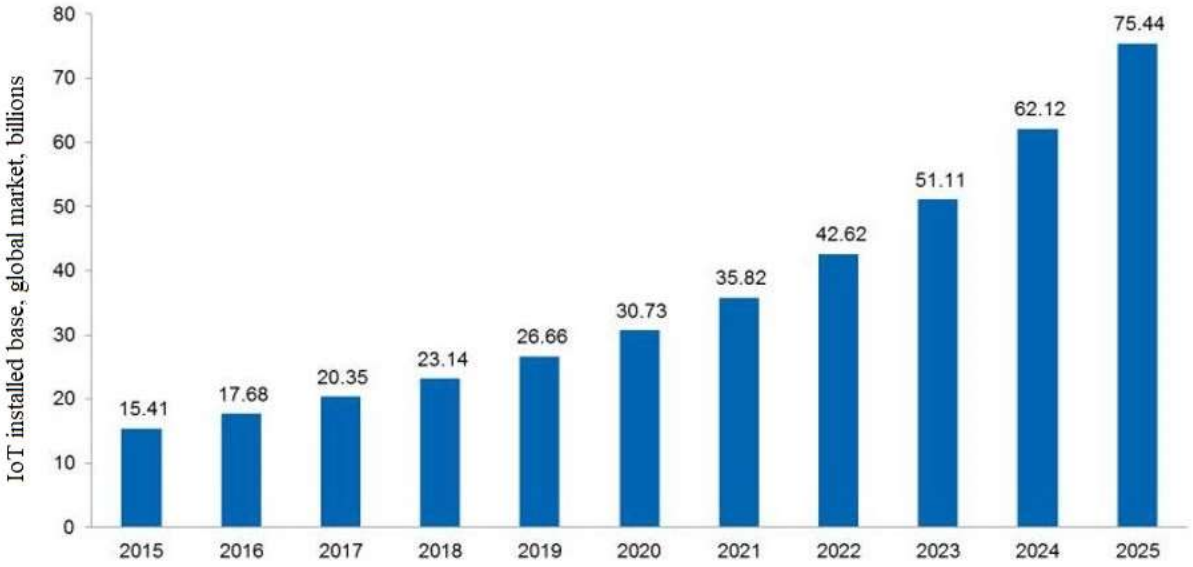

Fig. 1.1: Estimation of the IoT market [21].

With reference to Figure 1.2, the IoT is divided into short-range and long-range segments. Wi-Fi, Bluetooth, and ZigBee are available for short-range applications, and 2G/3G, 4G, 5G and Long Term Evolution (LTE) with extended range are considered as long-range categories. Additionally, a new low-power Wide-Area Network (LPWAN) is designed to provide long range at the expense of a low data rate. Short-range technologies demand high availability and low latency, with little regard for battery power consumption. In contrast, long-range technology is suitable for applications that need wide area coverage and extensive battery life.

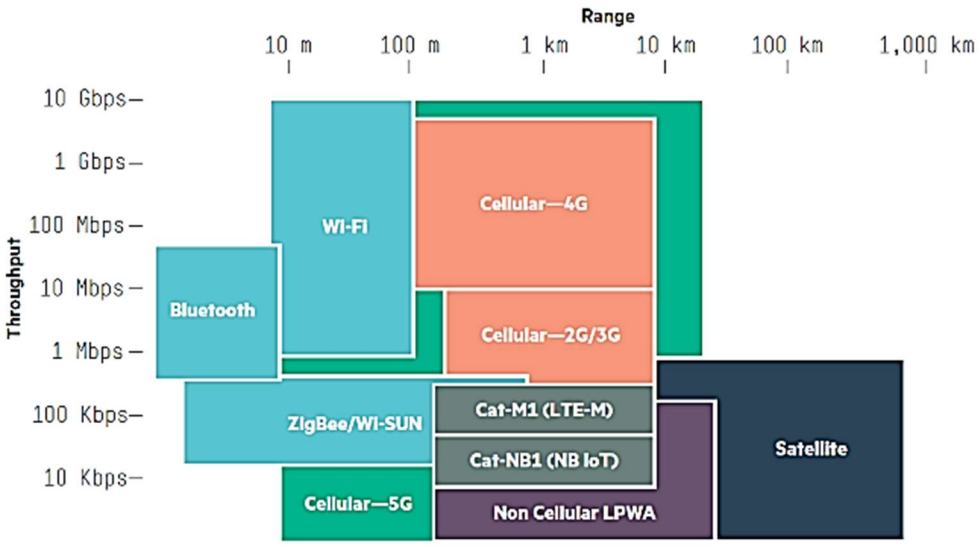

Fig. 1.2: Range and throughput of available wireless technologies [22].

LPWAN plays a vital role in this rapid growth and adoption of long-range IoT, and operates at both licensed and unlicensed frequencies. Operation at licensed frequencies guarantees security and Quality of Service (QoS) of the transmitted signal and operation at unlicensed frequencies provides a good coverage with low-cost service.

The report in [23] has identified that there is a growing research interest in IoT. As long-range IoT is new among IoT technologies, various aspects of it have not been extensively studied in real environments. Most research examines theoretical aspects of the technology. So far, limited work has been done on comparing the real-life performance of the long-range IoT to its theoretical performance. For example, most long-range IoT technologies claim a coverage area of ~10 km in rural and ~5 km in urban environments, but this is seldom achievable in most real life scenarios. The theoretical estimates given by the technology manufacturers are unreliable. This is because the performance depends on not only the type of environment but also the density of obstacles. Therefore, the overarching objective of this project is to study the performance of long-range IoT technologies in a real environment at the frequency of 915 MHz.

To do that, three main goals established for this study are to: (1) gather real-life empirical data on a particular Long-range IoT technology (LoRa) at Macquarie University, Sydney, Australia; (2) use this data to create numerical models to describe the propagation characteristics of LoRa in a real environment; and (3) estimate the worst-case coverage of the technology based on the introduced models.

(1) To accomplish the first goal, we have chosen the Macquarie University campus because it provides a diverse propagation environment, and a LoRa gateway is placed at one of the two possible locations on the campus. Its position is fixed while taking the measurements. We also located several end devices in different environments, where at each the received power is recorded.
(2) To accomplish the second goal, we use the stored data and develop single-frequency path-loss models for different propagation environments. Then, we compare these models and find the best one to predict the signal propagation.
(3) For the third goal, the proposed model is used to predict the coverage area of the gateway. Then we study the estimated coverage area in the real world.

1.2. Thesis Overview

This thesis consists of six chapters. The first chapter includes this introduction while the second chapter reviews the necessary background in the field of the Internet of Things. In Chapter 3, the principle of propagation mechanisms and some path-loss models are described. The components and methods used are discussed in Chapter 4. This chapter also presents the details of the related assumptions and solution approach used to find the path-loss models. Chapter 5 contains our main experimental results followed by a detailed discussion about different methods to predict LoRa's performance. Finally, Chapter 6 provides a conclusion and suggests some topics for future research.

Chapter 2
Literature Review

In this chapter, we review the wireless technologies for IoT applications that are suitable for long-range applications. The first part describes the potential of the long-range technology LPWAN. In the next two sections, we summarise the research carried out over the last decade on licensed and unlicensed communication technologies.

2.1. Long-range Technologies in the IoT

Short-range technologies are the most appropriate technologies in the IoT, but these technologies are not well suited for all applications. Some applications such as smart metering need low consumption levels and cost, but require long-distance or long-range IoT communication. Long-range technologies are considered to be solutions for filling this gap.

Long-range technology, with the pioneer of LPWAN, represents a novel technique to complement short-range IoT and provide a much wider range of IoT applications. Low data rate, low cost, long battery life and wide coverage area are characteristics of LPWAN. Furthermore, it can support a massive number of devices [24] (Figure 2.1). In this technology, a massive number of nodes transmit data through gateways to the Cloud for storage and use by consumers (Figure 2.2).

LPWAN technologies are optimised to offer a wide area coverage by improving the gain up to 20 dB compared to legacy cellular systems [25]. This allows end devices that are 10 kilometres from the network to connect to base stations. LPWAN is also suitable for operation in challenging indoor environments such as basements [26].

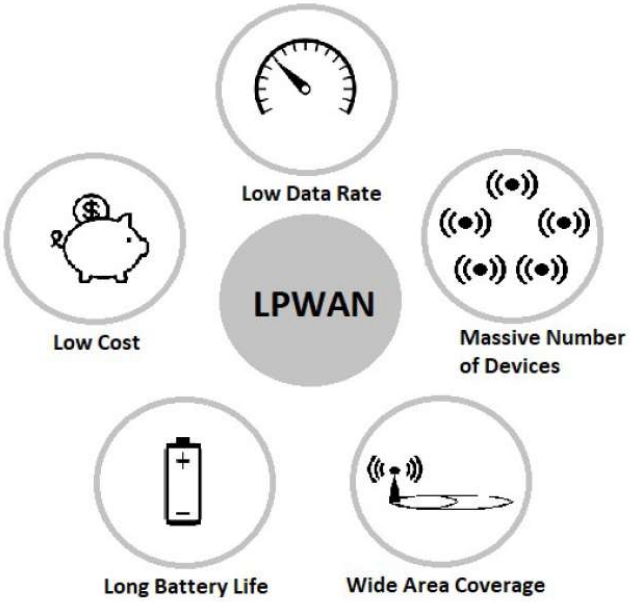

Fig. 2.1: Schematic diagram of the characteristics of LPWAN.

Minimising energy and power consumption in IoT devices is critical in extending the network lifetime. Different power-saving and power-management methods are already implemented in current deployments [27, 28]. For example, a star topology is used instead of a mesh topology in LPWAN technology. In [28, 29], turning off devices during periods of inactivity was proposed as a power-saving method. Here, the devices switch from the OFF state to ON upon arrival of new data. Other effective solutions for this issue are delegating complex tasks from end devices to the base stations, and using multiple channels or orthogonal signals simultaneously [30]. All these techniques help to preserve battery life for up to 10 years [31].

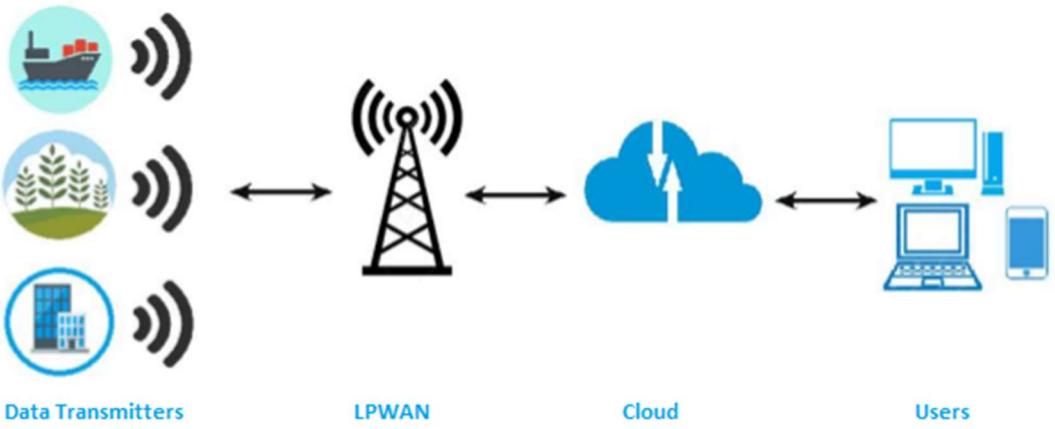

Fig. 2.2: Schematic diagram of an overview of the communication of LPWAN.

The demand for the IoT is increasing, but if LPWAN is to reach wider adaption, it needs to use low-cost devices to retain its hold on the market. To reduce cost, LPWAN offers various solutions such as: 1) simplifying the complexity of the processeing hardware to develop the system; 2) using unlicensed spectrum including the industrial, scientific and medical (ISM) band or TV white spaces; 3) sharing cellular bands to avoid the additional licensing cost. Any of these solutions has corresponding advantages and disadvantages, which are explained in the following section using licensed spectrum and unlicensed spectrum in LPWAN.

2.2. Licensed Spectrum

LPWAN utilises the licensed spectrum for applications that need capacity, scalability, security and regulatory constraints. It provides three solutions standardised by the 3rd Generation Partnership Project (3GPP) in its Release 13 [32]. These solutions are Long Term Evolution Machine Type Communications Category M1 (LTE MTC Cat M1), Extended Coverage GSM for the Internet of Things (EC-GSM IoT) and Narrowband IoT (NB-IoT), which are discussed in the following.

2.2.1. LTE MTC Cat MI

LTE MTC Cat M1 or LTE-M is an IoT technology that connects devices to the 4G network without a gateway and batteries. It provides lower device complexity and extended coverage by reusing current LTE base stations. It co-exists with 2G, 3G, and 4G mobile networks and benefits from all the security and privacy features of mobile networks.

Narrowband technology is used in LTE-M to provide bi-directional communication with a data rate of 1 Mbps and a link budget of 156 dBm. It utilises FDMA modulation for the uplink and OFDMA 16 QAM modulation for the downlink. The Cellular IoT (CIoT) plane and Evolved Packet System (EPS) are additional solutions for its optimising data transmission [33]. Furthermore, LTE-M uses the power-saving mode (PSM) and extended Discontinuous Reception (eDRX) to achiev 10 years of battery lifetime for a broad range of uses [34].

2.2.2. EC-GSM-IoT

Extended coverage GSM IoT (EC-GSM-IoT) is operated in the GSM band and, based on eGPRS, can be deployed to existing GSM networks through a software upgrade [35]. It offers a 20 dB coverage improvement beyond the typical GSM coverage. This corresponds to achieving a

target maximum coupling loss (MCL) of 164 dB [25]. It can also provide low-complexity and low-energy devices with a 10-year battery life. It uses the 900-MHz frequency band and GMSK modulation to transmit messages at 70 kbps [36]. EC-GSM-IoT is very suitable for challenging environments, such as deep indoor basements or remote areas.

2.2.3. NB-IoT

NB-IoT is a narrow-band radio technology standardised by the 3GPP. This technology was developed to cover a broad range of IoT devices. NB-IoT focuses explicitly on low-cost devices, high reliability, high network security and low power consumption, with a 10-year battery life [32]. It is also supported by many types of mobile equipment and can function synchronously with these devices. This means a reduced likelihood that additional funding for existing towers or other sites will be required, and the operations will be minimally impacted.

NB-IoT is deployed in three different operation modes: Stand-alone, Guard Band and In-Band (Figure 2.3) [37]:

Fig. 2.3: Three deployment scenarios of NB-IoT [38].

i) Stand-alone operation: This mode uses any available spectrum, for example, a GSM channel 200 kHz wide, with a 10 kHz guard interval on both sides of the spectrum.

ii) Guard-band operation: It uses the resource blocks and an unused guard band of an LTE carrier without affecting its capacity. This is suitable for spectrum allocations that do not match the set of LTE system bandwidths.

iii) In-band operation: It utilises the resource blocks within a common LTE carrier and provides the most spectrum- and cost-efficient deployment of NB-IoT.

Based on these operation modes, it is clear that the stand-alone and guard-band scenarios can provide a better indoor coverage. Deploying the NB-IoT in the 700 MHz, 800 MHz, and 900 MHz frequency bands makes it an excellent choice for operators because these frequency bands provide

extensive coverage. Moreover, NB-IoT technology is also a good choice for the market since it uses FDMA with GMSK modulation, offering low power and low-cost devices [39].

Table 2.1 presents a brief comparison of the three 3GPP cellular LPWAN standards mentioned above.

Table 2.1: 3GPP Cellular LPWAN summary

Attribute	LTE-M (Rel. 13)	EC-GSM	NB-IoT
Frequency band	700-900 MHz	800-900 MHz	700-900 MHz
Data rate	375 kbps	70 kbps	20-65 kbps
Bandwidth	1.08 MHz	200 kHz	200 kHz
Range	<15 km	<15 km	<35 km
Mobility	Yes	Yes	No

Table 2.1 illustrates that all three standards use operating frequencies that are popular among mobile operators, and they work at a long range at the expense of a low data rate. EC-GSM and NB-IoT utilise a narrow band for transmitting data, helping them to resist noise. Finally, LTE-M (Release 13) and EC-GSM can be used for mobile devices, while NB-IoT is suitable for fixed devices [40].

2.3. Unlicensed Spectrum

One of the major problems in the licensed spectrum is an expensive licensing fee. Hence, it is attractive to develop a long-range LPWAN for the unlicensed spectrum. Although the quality of service and the security of data are adversely affected, the installation price of this technology is significantly lower. The unlicensed spectrum technologies are usually deployed in ISM bands centred at 2.4 GHz, 868/915 MHz, 433 MHz, and 169 MHz, depending on the region of operation. The more popular unlicensed spectrum technologies are discussed in the following:

2.3.1. SIGFOX

The SIGFOX technology [41] was founded in 2009 and aims to send small amounts of data across the Internet. This technology employs Binary Phase Shift Keying (BPSK) as Ultra Narrow Band (UNB) modulation with a bit rate of 100 bps for uplink and a GFSK scheme operating at 500 bps on a 600 Hz spectrum segment for downlink. By using UNB, SIGFOX utilises bandwidth efficiently and experiences very low noise levels and low power consumption. Furthermore, this

attribute provides a higher receiver sensitivity and reduces the cost of antenna design. Only uplink communication was supported in the first version of SIGFOX technology, while in its updated versions downlink communication is also supported. On average, the technology can send 140 messages of 12 bytes per day and four messages of 8 bytes per day over uplink and downlink, respectively. This technology also claims that it can support one million connected devices in a network with a 30–50 km coverage in rural areas and 3–10 km coverage in urban areas. SIGFOX is not an open protocol and is limited to SIGFOX networks.

2.3.2. Long-range IoT Technology (LoRa)

LoRa is a physical-layer technology that transmits signals in the sub-GHz ISM band (868 MHz, 915 MHz, and 433 MHz) [42]. Using lower frequencies than the typical ISM bands (2.4 or 5.8 GHz) enables it to cover a wide area, especially when the nodes are within buildings [43, 44]. Instead of using narrowband transmission, it employs a form of spread-spectrum modulation, Chirp Spread Spectrum (CSS) [45]. CSS modulation spreads out information over different frequency channels and data rates [46]. This modulation uses linear frequency chirps over time to encode information that makes LoRa immune to interference caused by the Doppler Effect and echoes [47]. The signals transmitted have noise-like properties which are difficult to detect or jam [48]. This means that signals are robust against signal degradation such as interference and multipath fading. The LoRa system uses different Spreading Factors (SF) from 7 to 12 to support different data rates (from 0.3 kbps to 37.5 kbps). This system can transmit data from different channels simultaneously through different spreading factors [49].

A LoRa network typically utilises the star-of-star topology [46], in which gateways transmit data from end devices to a central network (Figure 2.4). Each gateway can independently support tens of thousands of end devices [46]. All gateways are connected to the network server via standard IP connections while the end devices use single-hop communication for sending data. All communication is bidirectional, and all transmitted messages from end devices are received by all base stations. These multiple receptions are resolved by the use of a Time Difference Of Arrival (TDOA) based localisation technique supported by very accurate timing [50].

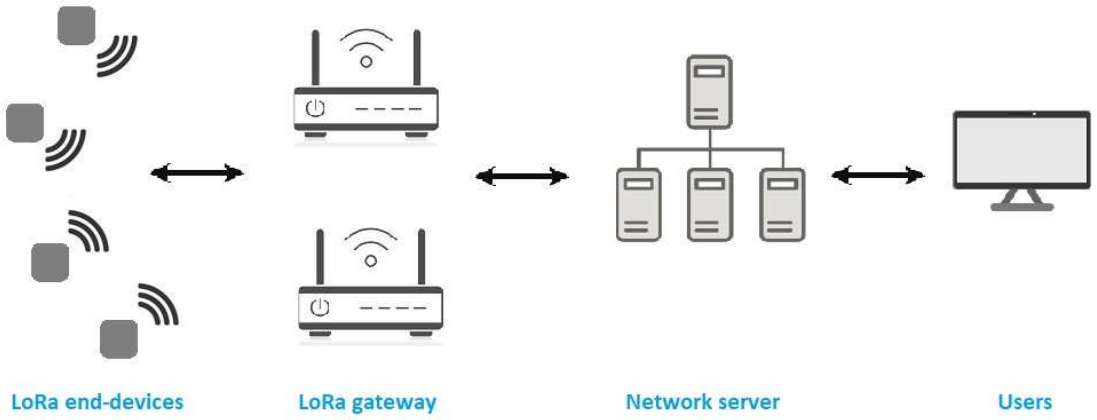

Fig. 2.4: LoRa network

A LoRa network can be categorised into three classes based on MAC layers [51]: Class A, Class B, and Class C. All of these support bi-directional communications but have different downlink capability.

i) Class A: This class is usually used by low-power end-device applications. Each end-bdevice's uplink transmission is followed by two short downlink receive windows (Figure 2.5). It transmits data at any time to the gateway, then listens to the gateway for a window of 1 and then 2 seconds for any downlink message. After that, it goes to sleep until the next transmission.

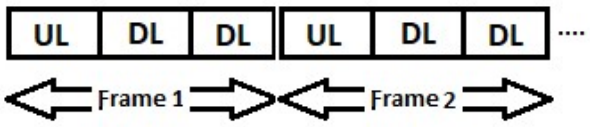

Fig. 2.5: Class A of LoRa technology.

ii) Class B: This class of LoRa receives windows during a downlink period additional to those of Class A (Figure 2.6). A Class B device receives a time-synchronised beacon from the gateway to indicate to the server when the end device is listening.

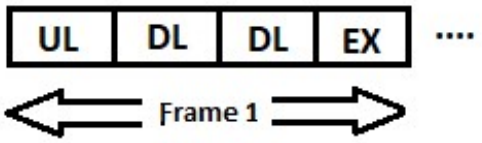

Fig. 2.6: Class B of LoRa technology.

iii) Class C: This class of end devices is used for AC-powered applications where sufficient power is available and, therefore, there is no need to minimise reception-time windows. A Class C device continuously listens for downlink messages except to transmit a mode (Figure 2.7). Furthermore, this class provides the lowest latency among all the LoRa classes.

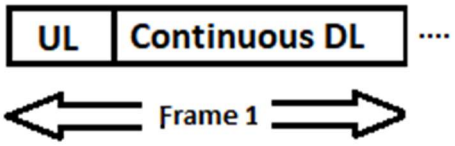

Fig. 2.7: Class C of LoRa technology.

In addition to the different classes in the MAC layer, LoRa uses the physical layer to transmit data. The LoRa packet format, which is specified in Semtech's transmitters and receivers [52], is shown in Figure 2.8.

The LoRa packet begins with preamble symbols used to signal the start of LoRa data, followed by an optional header. This header is transmitted with a Code Rate (CR) of 4/8 and indicates the payload length. After the payload, there is a 16-bit cyclic redundancy check (CRC) at the end of the transmission. LoRa utilises dual optional CRC frame structures, one in the header structure and another one at the end of the frame, to improve the architecture of the structure.

The important parameters which customise the LoRa modulation are: Spreading Factor (SF), Code Rate (CR) and Bandwidth (BW). These parameters determine LoRa's resistance against interference and ease of decoding. In the following, these parameters will be explained in more detail:

The Spreading Factor (SF) is a parameter that defines the length of the LoRa packet and varies from 7 to 12 [49]. LoRa employs different SFs to transmit data over different channels simultaneously. Spreading factors are orthogonal to each other and do not cause collisions. The value of the spreading factor tells how many chips are used to transmit one symbol. For example, with an SF of 7 (SF7), $2^7 = 128$ chips/symbol are used and with SF12, $2^{12} = 4096$ chips/symbol. Each increment in SF doubles the transmission duration and consequently increases the energy consumption. Furthermore, any rise in SF directly increases the LoRa modulation sensitivity and time on air [52].

a)

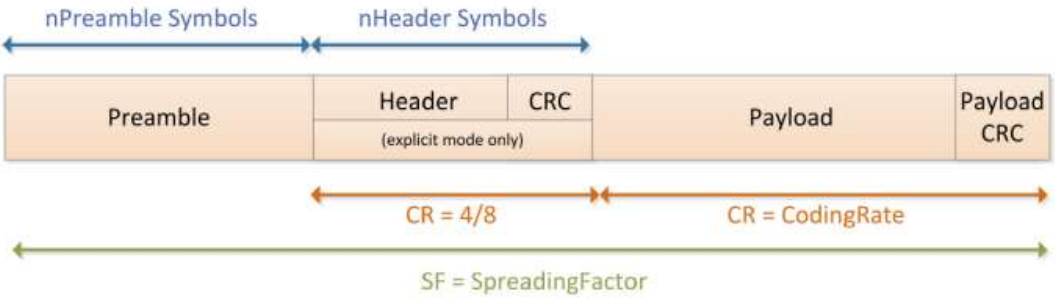

b)

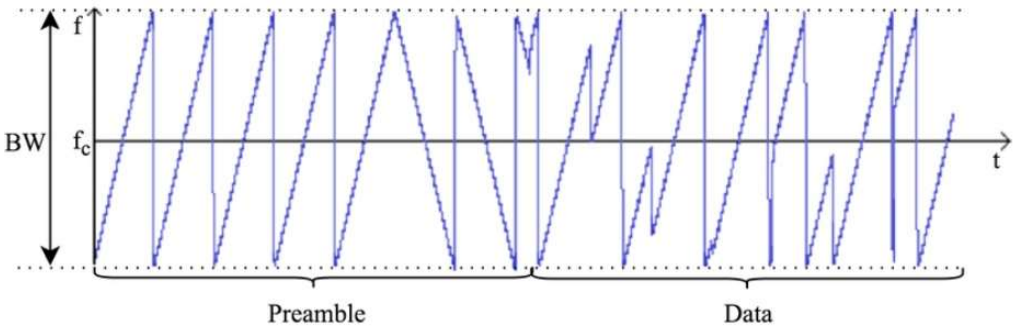

Figure 2.8: a) LoRa packet structure [52]. b) An example of a LoRa symbol with 8 up-chirp symbols for the preamble.

Bandwidth (BW), as another important parameter, is the range of the frequencies in the transmission band. Typical bandwidths in LoRa are 125 kHz, 250 kHz and 500 kHz If BW increases, the data rate increases and, consequently, the time on air and sensitivity decrease [52].

Another parameter that influences LoRa transmission quality is the Code Rate or CR. CR is the Forward Error Correction (FEC) rate that offers protection against interference and can be set to either 4/5, 4/6, 4/7 or 4/8. An LoRa modulation with a high CR increases robustness as well as time on air.

The parameters influencing LoRa receiver sensitivity are SF and BW [53]. As presented in Table 2.2, the lowest sensitivity is obtained with the minimum bandwidth (125 kHz) and the maximum spreading factor (SF12), while the highest value is obtained with a bandwidth of 500 kHz and spreading factor of 7.

Table 2.2: LoRa receiver sensitivity (dBm) for different spreading factors and bandwidths.

	SF12	SF11	SF10	SF9	SF8	SF7
BW=500 kHz	-130	-129	-127	-124	-121	-118
BW=250 kHz	-134	-133	-131	-128	-125	-122
BW=125 kHz	-137	-136	-134	-131	-128	-125

2.4. Chapter Summary

In this chapter, we review LPWAN as a new technology in long-range IoT and divide it into two categories. Firstly, licensed-spectrum technologies that re-use existing cellular sites for sending messages and are very secure and reliable but whose service and spectrum cost are high. EC-GSM-IoT, LTE-M and NB-IoT are the technologies which operate in the licensed-spectrum band. Secondly, unlicensed-spectrum technologies that use the sub-GHz ISM band to reduce the cost at the expense of security. The two popular technologies of this category are SIGFOX and LoRa.

Chapter 3
Signal Propagation

This chapter gives basic information about the received signal power and the signal propagation that is used in the project. Firstly, we describe the various propagation environments between the transmitter and the receiver. Then, we explain the received power strength and sensitivity. Finally, we present a theoretical overview of existing propagation models.

3.1. Environment Type

In wireless communication, there are two propagation environments: Line-of-Sight (LOS) and Non-Line-of-Sight (NLOS). We call the propagation environment is LOS if there is a direct visual path (or line of sight) between the transmitter and the receiver. This means that there are no obstacles in the path between the transmitter and the receiver. NLOS is a term often used when there is no visual line of sight between the transmitting antenna and the receiving antenna. Obstacles that cause NLOS conditions are buildings, trees, hills, mountains and high-voltage power lines.

3.2. Received Signal Strength Indicator (RSSI)

The Received Signal Strength Indicator (RSSI) is the power of received signal in dB. It can be calculated as follows:

$$P_{rx} = P_{tx} + G_{tx} - L_{tx} - L_{pl} - L_m + G_{rx} - L_{rx} \quad (3.1)$$

where P_{rx} is RSSI in dB, P_{tx} is the transmitted power in dB, G_{tx} is the transmitter antenna gain in dBi, L_{tx} is the transmitter loss in dB, L_{pl} is the path loss in dB, L_m shows the fading margin in dB, G_{rx} is the receiver antenna gain in dBi and L_{rx} are the receiver losses in dB and it can be summarised as:

$$P_{rx} = P_{tx} + G_{tx} + G_{rx} - L_{pl} \tag{3.2}$$

where L_{pl} represents the general path loss determined by the nature of the communication environment.

3.3. Receiver Sensitivity

The receiver sensitivity is one of the vital specifications of wireless communications and is defined as the ability of the radio receiver to pick up the required level of radio signals. The receiver sensitivity is the minimum magnitude of input signal required to be successfully detected by the receiver. The lower the sensitivity level, the more effective the receiver is at detecting received signals. For example, a receiver can detect more RF signals and demodulate them with a −100 dBm sensitivity than with a −90 dBm sensitivity.

Generally, the admission of a transmitted signal by a receiver can be formulated as follow:

$$A = \begin{cases} 1 & P_{rx} > S_{rx} \\ 0 & P_{rx} \leq S_{rx} \end{cases} \tag{3.3}$$

where P_{rx} is the received power and S_{rx} is the receiver sensitivity.

3.4. Propagation or Path Loss

The radio propagation loss or path loss is the degradation in the received power of an electromagnetic signal when it travels from the transmitter to the receiver. Path loss is due to several effects such as Free Space loss, reflection, scattering, diffraction, and absorption. Furthermore, the path loss is influenced by the environment (urban or rural) and the propagation medium (dry or moist air). The signal radiated by a transmitter may also take different paths to reach to a receiver. This effect is called multipath which results in either an increase or a decrease of the received signal level. In the following, each factor is defined in more detail:

1) *Reflection*: reflection occurs when a wave impinges upon smooth objects such as the earth and walls (Figure 3.1.a).
2) *Scattering*: it occurs when a transmitted signal impinges on an object that causes the reflected energy to spread out in many directions (Figure 3.1.b).
3) *Diffraction*: diffraction occurs when the transmitted signal impinges on objects with a sharp edge (Figure 3.1.c).

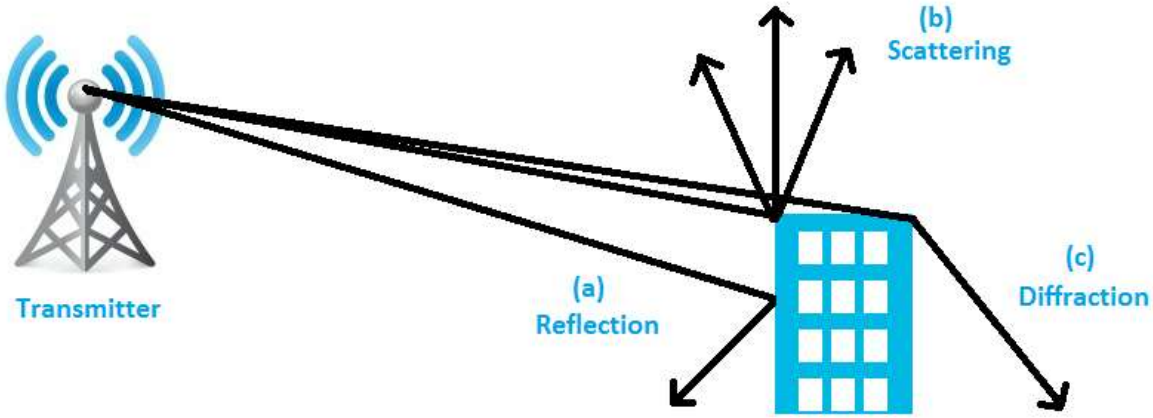

Figure 3.1: Reflection, Scattering and Diffraction.

4) *Multipath loss*: it occurs when multiple waves arrive at the receiver. Multipath propagation causes large and rapid fluctuations in signal strength.
5) *Absorption loss*: it occurs when the radio signal passes into mediums which are not totally transparent to radio signals. These mediums can be buildings, walls, furniture as well as vegetation and atmosphere moisture.

3.5. Path-Loss Models

For a wireless communication system, the ability to predict radio propagation behaviour and the coverage area of a base station is very important. Since site measurements are expensive, path-loss models have been developed as low cost and convenient alternatives to estimate signal propagation. There are many path-loss models available which can be categorised into three main types: empirical models, deterministic models, and stochastic models [54].

Empirical models are based on observations and measurements. These models are mainly used to predict the behaviour approximately. They can be split into two subcategories, namely time-dispersive and non-time-dispersive [55]. The time-dispersive group provides information

regarding the time-dispersive characteristics of the channel, for example the multipath delay spread of the channel. The Stanford University Interim (SUI) model for a carrier frequency (f_c) above 2 GHz [56] is a perfect example of this type, and the COST 231-Hata model and the Okumura-Hata model for f_c below 2 GHz [57] are the most commonly used models of a non-time-dispersive empirical type. All these models predict the path loss as a function of various parameters such as distance and antenna height.

Deterministic models use the physical laws of wave propagation to determine the received signal power at a particular location. These models depend on a detailed and accurate 3-D map of the propagation environment and may be expected to predict path loss more accurately than the empirical methods but with more computation effort. An example of this type is a raytracing model [58].

Stochastic models use a series of random variables to model the environment. These models are the least accurate models among the path-loss models but require the least information about the environment and use much less processing power to generate predictions.

Keeping in view the ease of implementation we focus on empirical models. We consider the Free-Space Path-Loss (FSPL) model as the reference model for all path-loss estimation.

3.5.1. FSPL Model

This model estimates the signal attenuation when the transmitter and receiver have a clear line-of-sight path with no obstacles nearby to cause reflection or diffraction. FSPL is proportional to the square of the transmitter-receiver (T-R) separation distance (Figure 3.2), and is also proportional to the square of the carrier frequency, according to [59]:

$$\mathrm{FSPL} = \left(\frac{4\pi d f_c}{c}\right)^2 \tag{3.4}$$

where f_c is the signal frequency in Hz, d is the distance between transmitter and receiver in m, and c is the speed of light in a vacuum. In terms of dB (3.4) becomes:

$$\mathrm{PL}^{\mathrm{FSPL}} = 20\log_{10}(d) + 20\log_{10}(f_c) + 20\log_{10}\left(\frac{4\pi}{c}\right) \tag{3.5}$$

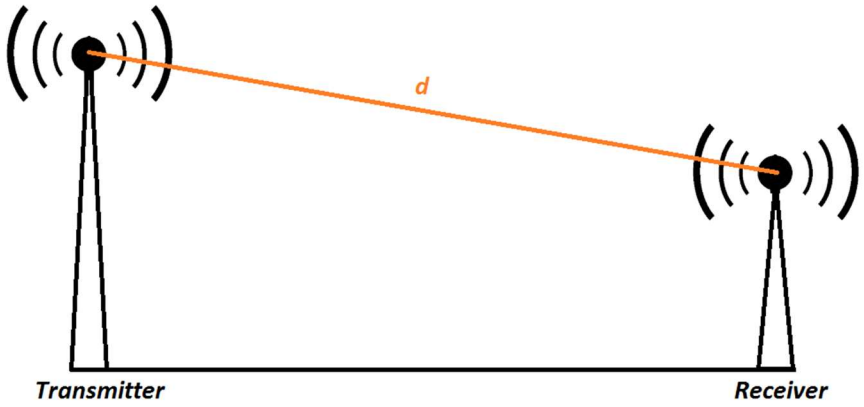

Figure 3.2: Transmitter-Receiver separation distance

3.5.2. Okumura-Hata Model

The Hata model is an empirical formulation of graphical information from the Okumura model that shows the effects of diffraction, reflection, and scattering caused by city structures. It is valid in the range from 150 MHz to 1500 MHz. The mathematical expression of this model is as follows [57]:

$$\mathrm{PL} = \begin{cases} A + B\log_{10}(d) & for\ urban\ areas \\ A + B\log_{10}(d) - C & for\ suburban\ areas \\ A + B\log_{10}(d) - D & for\ open\ areas \end{cases} \tag{3.6}$$

$$A = 69.55 + 26.161\log_{10}(f_c) - 13.82\log_{10}(h_b) - a(h_m)$$

$$B = 44.9 - 6.55\log_{10}(h_b)$$

$$C = 5.4 + 2[\log_{10}(f_c/28)]^2$$

$$D = 40.94 + 4.78[\log_{10}(f_c)]^2 - 18.33\log_{10}(f_c)$$

where $a(h_m) =$

$$\begin{cases} [1.1\log_{10}(f_c) - 0.7]h_m - [1.56\log_{10}(f_c) - 0.8] & for\ medium\ or\ small\ cities \\ 8.29\,[\log_{10}(1.54\,h_m)]^2 - 1.1 & for\ large\ cities\ and\ f_c \leq 200\ \mathrm{MHz} \\ 3.2\,[\log_{10}(11.75\,h_m)]^2 - 4.97 & for\ large\ cities\ and\ f_c > 200\ \mathrm{MHz} \end{cases}$$

f_c is the carrier frequency in MHz, d is the distance between transmitter and receiver antennas in km, h_b is the transmitter antenna height (above ground) in m and h_m is the receiver antenna height in m.

3.5.3. COST 231-Hata Model

The COST 231-Hata model was initiated as an extension of the Hata model. It is used to calculate the path loss in three different environments like urban, suburban and rural (flat). The basic path-loss equation for this COST 231-Hata Model can be expressed as [60]:

$$\mathrm{PL} = 46.3 + 33.9\log_{10}(f_c) - 13.82\log_{10}(h_b) - ah_m + \left(44.9 - 6.55\log_{10}(h_b)\right)\log_{10}(d) + c_m \tag{3.7}$$

where f_c, d and h_b are parameters defined in the Okumura-Hata model. The parameter c_m is equal to 0 dB for suburban and open environments and 3 dB for urban areas. The parameter ah_m is defined for urban areas as

$$ah_m = 3.2\,(\log_{10}(11.75\,h_r))^2 - 4.97, \quad \text{for } f_c > 400 \text{ MHz}$$

and for suburban and open areas as

$$ah_m = (1.1\log_{10}(f_c) - 0.7)h_m - (1.56\log_{10}(f_c) - 0.8)$$

where h_m is the effective height of the receiver in m.

3.5.4. Close-in (CI) Model

The single-frequency close-in (CI) model, which is known as a common-path-loss model, is defined by [61]:

$$\mathrm{PL}^{\mathrm{CI}}(f_c, d)[dB] = 20\log_{10}\left(\frac{4\pi f_c}{c}\right) + 10n\log_{10}\left(\frac{d}{d_0}\right) + X_\sigma^{\mathrm{CI}} \tag{3.8}$$

for $d \geq d_0$, where $d_0 = 1$ m, f_c is the frequency in Hz, n denotes the path-loss exponent (PLE), d is the distance in m. X_σ^{CI} is the zero-mean Gaussian random variable with standard deviation σ in dB and represents large-scale shadow fading. n in this model is found by minimising σ via the minimum mean-square-error (MMSE) approach. The expression for minimising the σ can be found in Appendix A.

3.5.5. Floating-intercept (FI) Model

The floating-intercept (FI) model is another candidate for a path-loss model. This model has two parameters and the equation for the FI model is given as [61]:

$$\mathrm{PL}^{\mathrm{FI}}(d)[\mathrm{dB}] = \alpha + 10\beta\log_{10}(d) + X_{\sigma}^{\mathrm{FI}} \tag{3.9}$$

where α is the floating intercept in dB, β denotes the slope of the line, X_{σ}^{FI} represents the large-scale shadow-fading variable and d is the 3D T-R separation distance in m. The parameters α and β are obtained through the least-squares linear fitting method to minimise the standard deviation σ of the shadow fading.

3.6. Chapter Summary

In this chapter, we explain the signal propagation between transmitter and receiver and the models used for signal-propagation estimation. The models are generally categorised into three types: empirical, deterministic and stochastic. Empirical models are based on observations and measurements and give accurate results. Deterministic models use basic physical approaches according to existing knowledge and require a complete 3-D map of the propagation environment. Stochastic models, the least accurate models, use a series of random variables to model the environment. Our focus in this chapter was on empirical path-loss models, namely the FSPL model, the Okumura-Hata model, the COST 231-Hata model, the CI model and the FI model.

Chapter 4
Methodology for LoRa Performance

An accurate analysis of LoRa's performance can be achieved by a good understanding of the instruments, measurement and analysis methods. Therefore, this chapter provides information about the components and techniques that were employed in the project.

4.1. Instruments Used

As the first step of the project, we create our LoRa network. The network consists of three main components: gateway or base station, end-devices and a network server.

4.1.1. Gateway

We use an LG01-S device as our gateway or base station (Figure 4.1). The LG01-S works as an open-source single-channel LoRa Gateway [62] to bridge end-devices to the LoRa Network Server via WiFi, Ethernet, 3G or 4G cellular. The frequency that is selected for the gateway is 915 MHz, as is specified for Australia [63].

4.1.2. End-Device

End-devices are nodes that send the measurements from sensors to the gateway. We use the Dragino LoRa Shield with a maximum +20 dBm power antenna connected to an Arduino Board (Figure 4.2) as our end-device. Each shield has five analogue ports and 13 digital ports.

Fig. 4.1: LG01-S as LoRa gateway

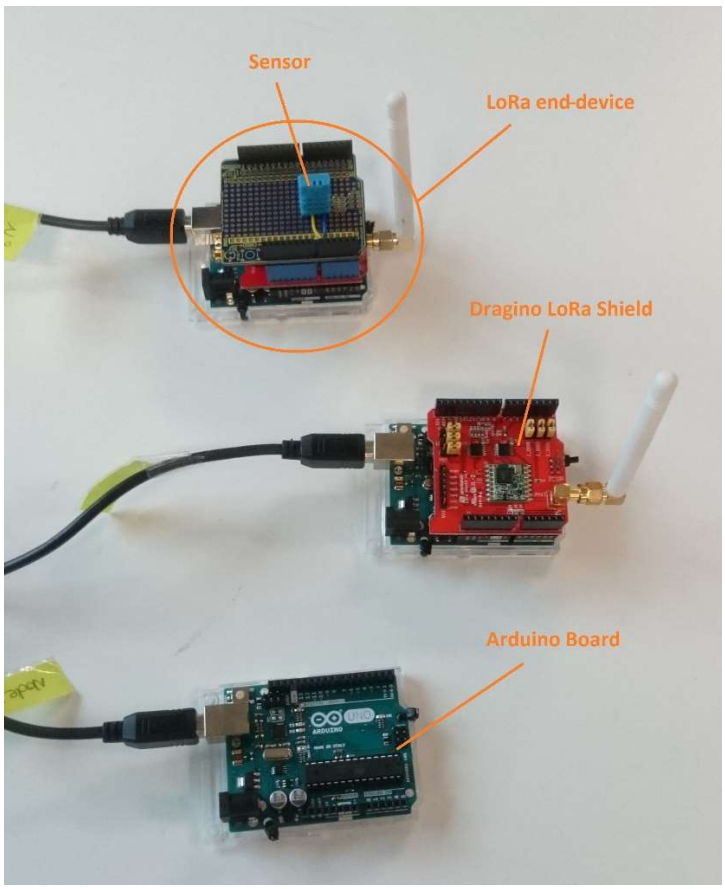

Fig. 4.2: Dragino LoRa Shield connected to Arduino Board for measuring data.

The antennas used in our project (both the gateway and the end-device) are helical antennas with the radiation pattern shown in Figure 4.3; this antenna is very similar to an omni-directional antenna.

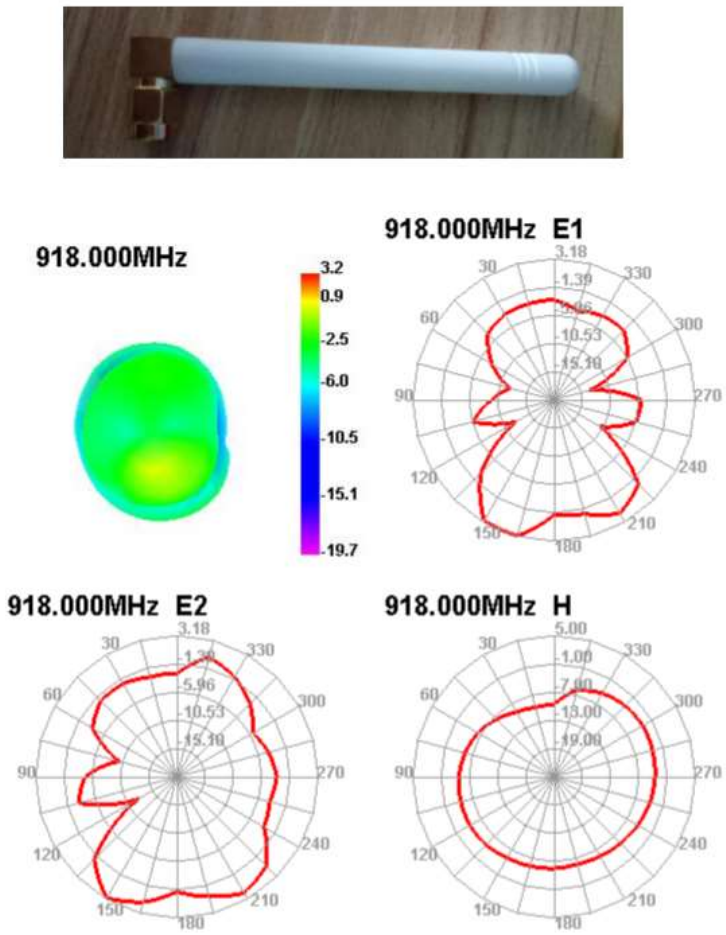

Fig. 4.3: Antenna used in the project and its radiation pattern.

4.1.3. Network Server

For the network server, “ThingSpeak” has been selected, due to its open source nature. It is used to upload data from the end-devices for further analysis [64] (Figure 4.4).

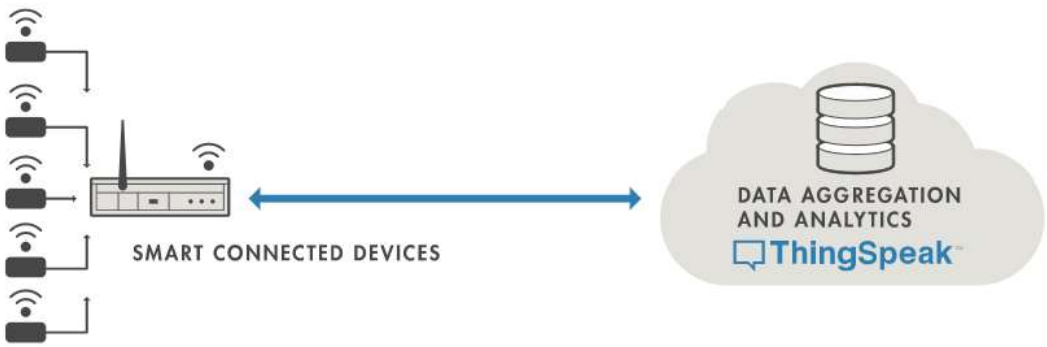

Fig. 4.4: ThingSpeak connection with the gateway [64].

4.1.4. Spectrum Analyser

Besides the above-mentioned components, we have also used an RSA306B USB spectrum analyser to monitor and study the captured signals (Figure 4.5). The RSA306B is a portable spectrum analyser that can be easily connected to an end-device like a personal computer, tablet or laptop via a USB port. This device uses a PC and Tektronix SignalVu-PC RF Signal Analysis software to provide low-cost real-time spectrum analysis. Since SignalVu-PC is a Windows-based application, it is readily accessible for users [65].

a)

b)

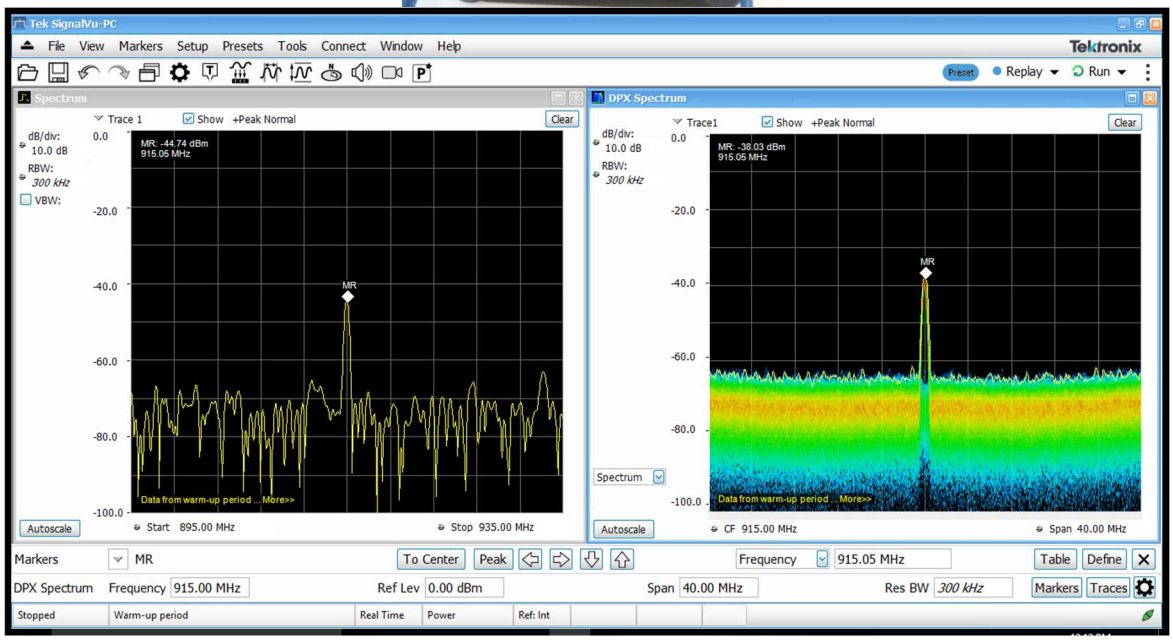

Fig. 4.5: a) RSA306B USB Tektronix spectrum analyser, b) Obtained signal and analysis by SignalVu-PC software

4.2. Measurement Environment

Experiments were conducted on the Macquarie University campus. We chose this location because it provides a diverse propagation environment. As Figure 4.6 shows, there is an open area that provides a good opportunity to analyse the Line-of-Sight (LoS) performance and the rest of the campus is available for analysing the Non-Line-of-Sight (NLOS) performance in rural and urban areas. Two transmitter (TX) locations and 50 receiver (RX) locations were selected, resulting in measurements from 60 T-R location combinations that had T-R separation distanceslo ranging from 20 m to 600 m, with RX locations in LOS and NLOS environments.

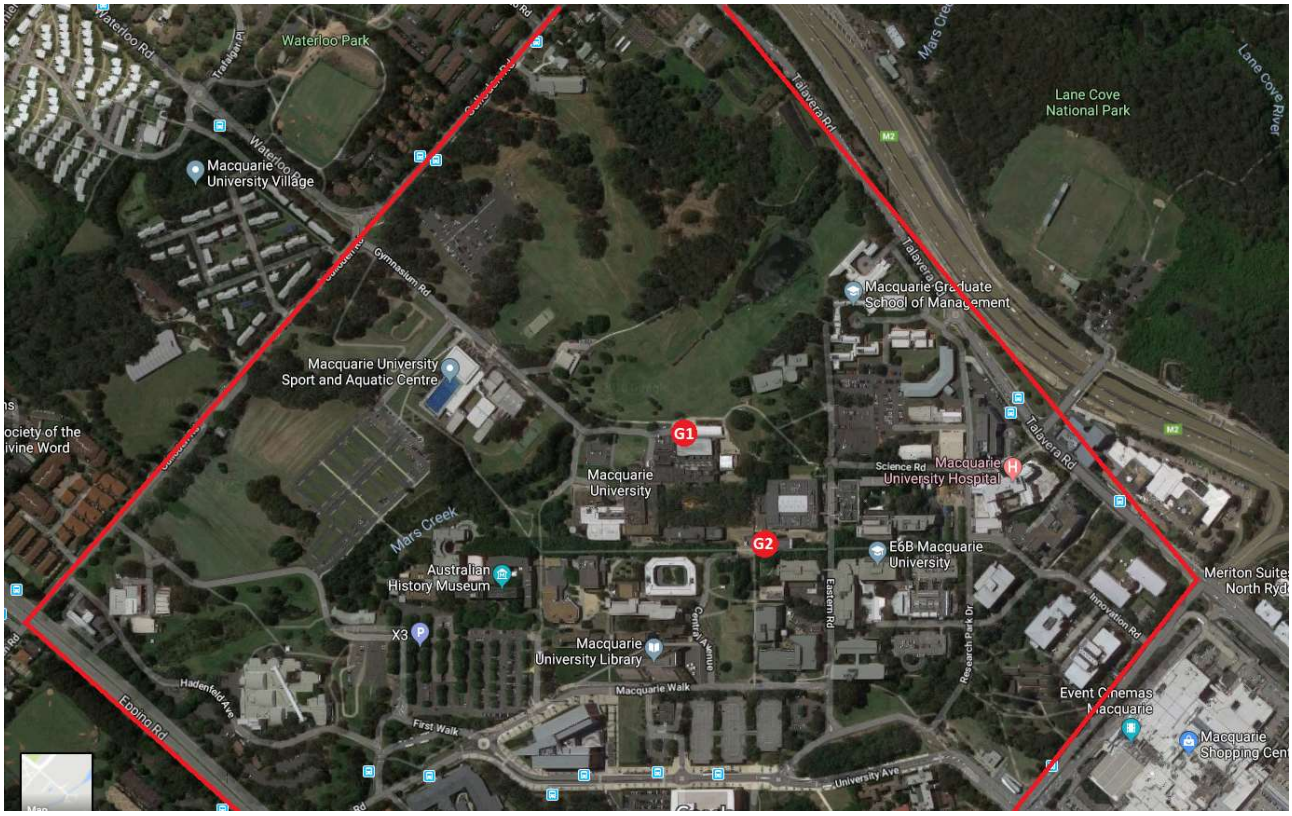

Fig. 4.6: Macquarie University campus

4.3. Experimental Procedure

The detailed procedure that we follow in this study to find propagation models for LoRa includes three steps: 1) Measurement and data collection; 2) Path-loss model comparison and introducing new models; 3) Coverage-area exploration.

4.3.1. Measurement and Data Collection

To develop a good empirical model, it is essential to configure the LoRa parameters to give us the maximum variable range of RSSI. According to Table 2.2 and equation (3.3), the received signal strength and sensitivity are influenced by parameters such as the spreading factor (SF), bandwidth (BW) and transmission power (P_{tx}), which should be adjusted before taking the measurements. In our experiment, we set the parameters as follows, SF to SF12, BW to 125 kHz and P_{tx} to 20 dBm. These parameters provide the highest received power and allows the lowest sensitivity. We set the frequency f_c to 915 MHz, which is part of the ISM band in Australia. We also keep the CR at its default value of 4/5.

After adjusting the parameters, the gateway was programmed to transmit a LoRa signal over the air periodically. We mounted the gateway on the 2nd floor of a two-storeyed building (point G1 in Figure 4.6), and the RSA306B (spectrum analyser) is placed at various points on campus for taking the measurements. Every time the gateway transmits a signal, RSA306B shows a pick-shape signal at frequency 915 MHz, along with the RSSI value.

RSA306B was able to detect the signal as long as the RSSI value was higher than the environment noise floor (-63 dB). The maximum distance that RSA306B was able to detect the LoRa's signal was ~15 m. This means that spectrum analyser is not suitable for RSSI measurement at long distances. Hence, we use a LoRa node instead of RSA306B for our experiments. Using Arduino Software, we programmed a LoRa node to send a message periodically to the LoRa gateway and to receive the acknowledgement (ACK), and record the RSSI value of ACK signal. (Codes are available in Appendix C, part 1).

In order to verify the reliability of the values measured by the LoRa node, these values are compared with those obtained by the spectrum analyser, RSA306B. The result of this experiment is presented in Figure 4.7. As the figure shows, the recorded signals have the same trend for both devices, although the signals are not matched due to the difference in specifications of the devices, such as the pattern and gain of the receiver antenna. Thus, Figure 4.7 shows that the values measured by the node device are reliable.

Next, the LoRa node was located in different parts of the campus. In each location, more than 10 individual snapshots of the received signal power were taken at intervals of 30 s and were stored

for further analysis. The same method was used when the gateway location moved to point G2, on top of an eight-storeyed building with an effective height of 27 m.

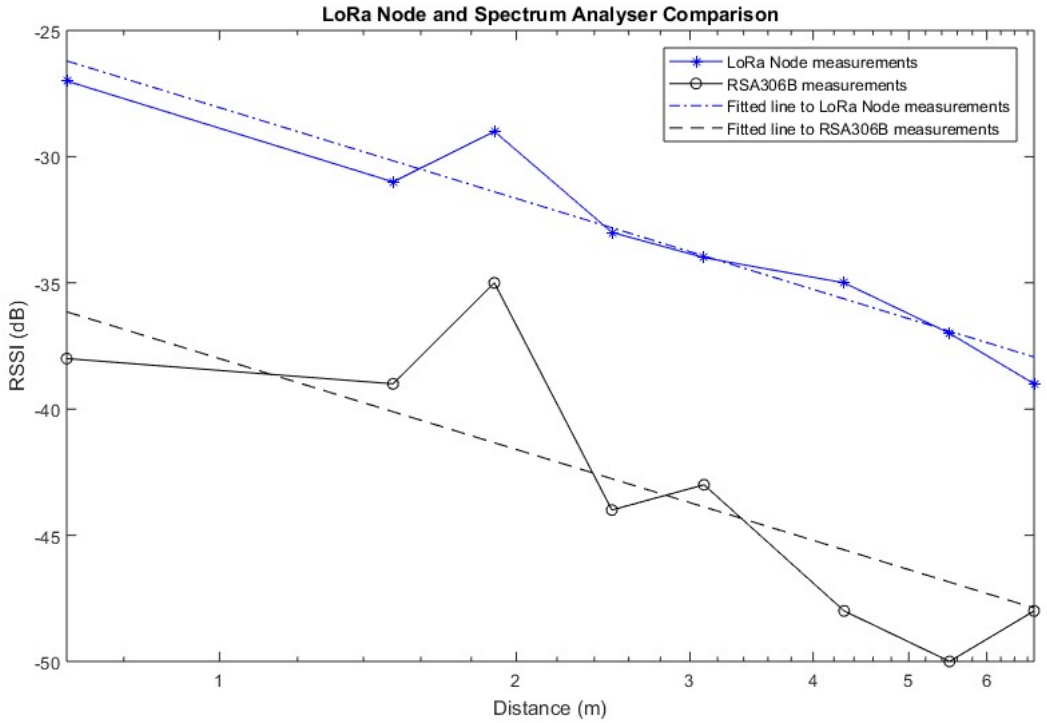

Fig. 4.7: Comparison between the RSSI values measured by the LoRa node and RSA306B.

4.3.2. Path-loss Model Comparison and Introducing New Models

In this step, the empirical measurements are compared with the most commonly used models, namely the FSPL model, the Okumura-Hata model and the Cost 231-Hata model. The comparison enables us to find the best-fitted model for each environment type. To do this, we use MATLAB and ICS telecom EV software.

ICS telecom EV is the most comprehensive radio planning tool, and allows users to model and simulate any radio technology from standardised technologies such as 3GPP and TETRA to emerging technologies such as IoT LPWAN. ICS telecom EV supports LoRa/LoRaWAN technology with seven different spreading factors (SF) and 4 coding-rate schemes. This software is equipped with the most comprehensive library of standard and specialized propagation models, across the whole radio frequency spectrum, including the Okumura-Hata model and the FSPL model. Models include diffraction, sub-path attenuation, troposcattering, ducting, reflections, refraction, absorption, and climate impact [66].

Besides the above-mentioned models we also use the close-in (CI) free-space reference distance path-loss model and the floating-intercept (FI) path-loss model to find the best-matched model for the recorded data.

4.3.3. Coverage-area Exploration

To find the coverage area, we use a star network in which LG01-S, as the network gateway, is mounted on the tallest building of the campus (point G2 in Figure 4.6) and LoRa nodes are distributed randomly in an area with a radius of 1.5 km. In this step, the nodes are programmed to send the temperature value measured by DHT11 sensors to ThingSpeak channels via the LG01-S (Figure 4.8). The code written for this purpose is presented in Appendix C, part 2. Analysis of the stored data enables us to find the LG01-S coverage area. Using the results of this step, we will attempt to find the most accurate path-loss model for coverage area estimation.

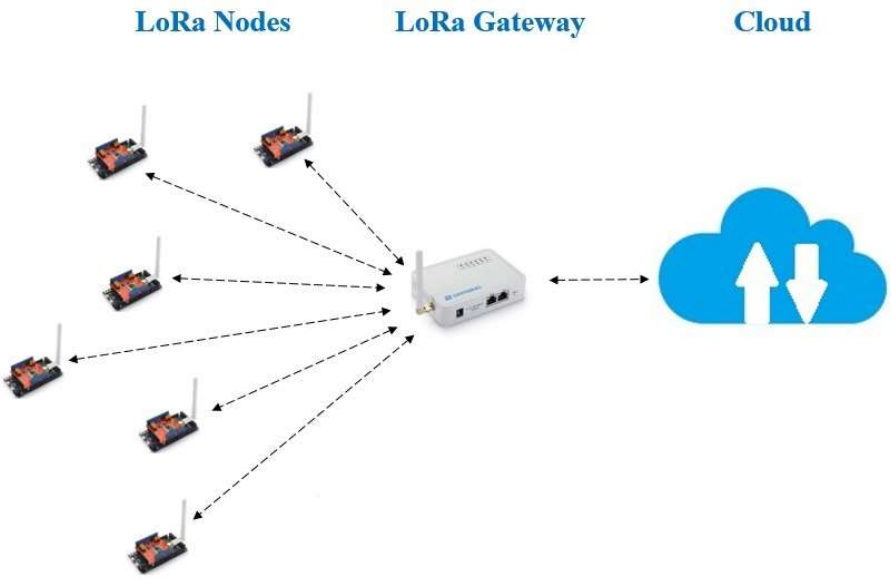

Fig. 4.8: The LoRa network

4.4. Chapter Summary

This chapter provides information about the instruments and parameter settings required to design a LoRa network. The procedure of measuring, and analysing the recorded data is also explained in this chapter as well as the required software code for each experiment.

Chapter 5
Results and Discussion

This chapter contains the analysis, presentation and interpretation of our measurements. Initially, we investigate the path-loss model to best estimate the recorded data in an open area, a rural area and an urban area. Then, the actual coverage area of the LG01-S will be found by analysing the data stored in the ThingSpeak channels. Finally, the actual value will be compared with the estimation of the proposed path-loss models.

5.1. Propagation in Open Area

To study the LoRa performance in an open area, two locations were considered for the gateway, point G1 and point G2 in Figure 4.6. During the measurements, the gateway was placed at a fixed position, while the receiver was moved to different locations on the campus. In total, over 320 measurements were recorded at more than 23 locations in the open area of the campus. At each location, more than 10 individual snapshots of the received signal power were taken at an interval of 30s and the strongest received power was selected in order to study the LoRa propagation. Table (B.1) in Appendix B presents the strongest value in each location of the open area. To achieve the propagation value we subtracted the transmitted power, antenna gains and antenna losses, which are in total +2 dB, from the recorded RSSI. Furthermore, it should be noted that the effective height of the transmitter was 10 m at G1 and 27 m at G2 while the effective height of the receiver was 10 cm.

To investigate the estimation of each path-loss model described in the previous chapter, we divided the path-loss models into two groups: 1) the models in which the transmitter and receiver antenna heights are considered, which included the Okumura-Hata model and the COST 231-Hata

model; 2) the models based only on the T-R separation distance such as the FSPL model, the CI model and the FI model.

Figure 5.1 illustrates the scatter plots of the measurements, the Okumura-Hata and COST 231-Hata models with two different base-station antenna heights $h_b = 10$ and $h_b = 27$ meters. As the figure shows, the COST 231-Hata model, in general, overestimates the path loss, especially at greater antenna height. The Okumura-Hata model with $h_b = 10$ under-predicts the path loss significantly, while this model with $h_b = 27$ better estimates the measured data.

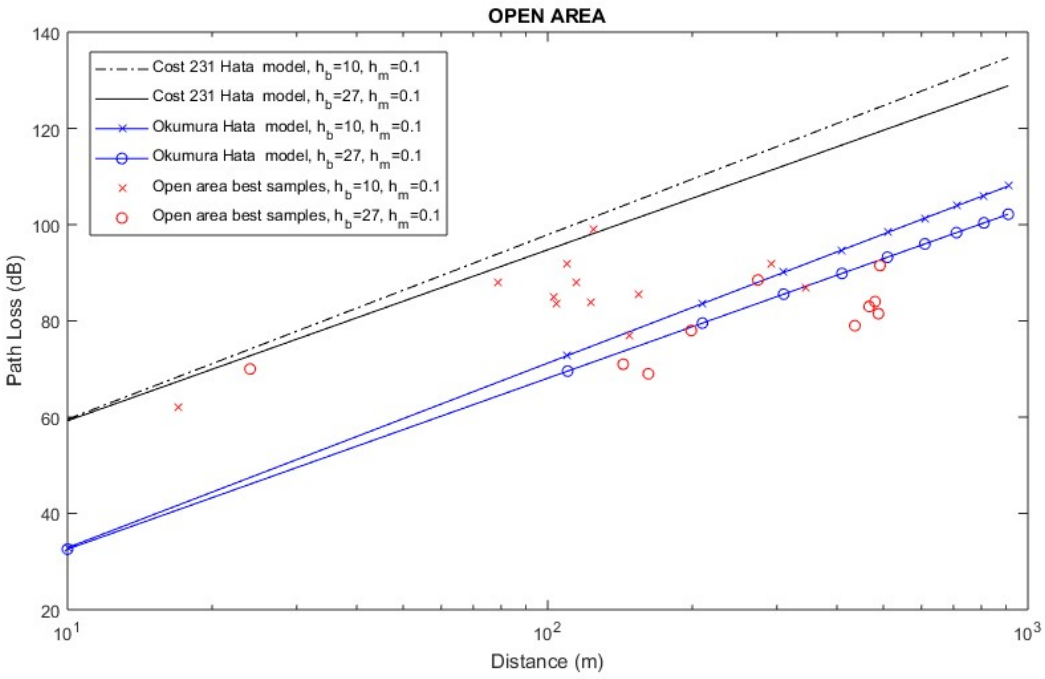

Fig. 5.1: Okumura-Hata model and COST 231-Hata model estimation for open-area measurements.

Figure 5.2 shows the predictions made using three models, namely the FSPL model, CI and FI models for various separation distances between transmitter and receiver. As is shown in the figure, the FSPL model under-predicts the signal propagation in this case while the two other models fit well with the measured data. The fitted models were obtained through the minimum mean-square error (MMSE) at each individual distance. The parameters of the FI model are $\alpha = 60.34$ and $\beta = 1$ and the PLE of the CI model is 2.27, which is higher than the theoretical free-space PLE of 2. This increase in PLE is the result of the fact that the open area of the campus is not a real free space and is surrounded by many obstacles such as buildings and trees, which cause much fluctuation in the measurements.

To find the best-matched model for the measurements, it is necessary to compare the error-estimation statistics of the models with each other. The mean prediction error, μ, and the standard deviation of the predicted error, σ, are two important factors for this purpose which are defined in (5,1) and (5.2), respectively.

$$\mu = \sum(\mathrm{PL}^{measured} - \mathrm{PL}^{model})\,/N \tag{5.1}$$

$$\sigma = \sqrt{\sum(\mathrm{PL}^{measured} - \mathrm{PL}^{model})^2\,/N} \tag{5.2}$$

where $\mathrm{PL}^{measured}$ and PL^{model} are the measured and predicted path loss, respectively, and N is the number of measurements.

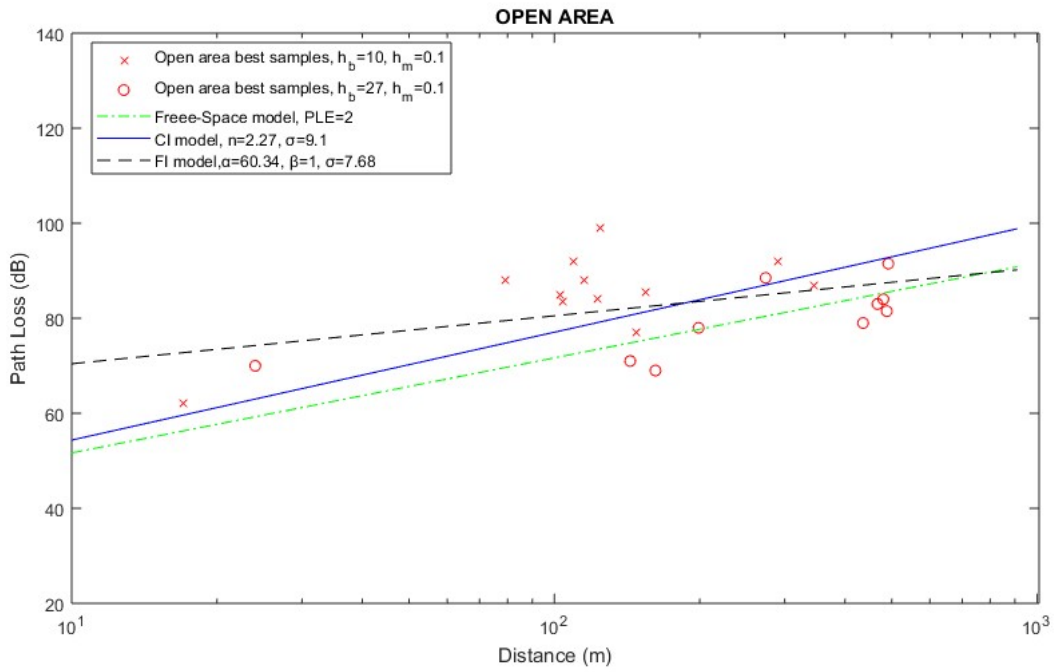

Fig. 5.2: FSPL model, CI model and FI model estimation for open-area measurments.

The corresponding error statistics of the path models are displayed in Table 5.1. Note that the prediction error is calculated as the difference between the measured value and the estimated value. Therefore, a significant negative mean value indicates that the model over-predicts the actual propagation. As is shown in the table, Cost231-Hata over-estimates the measurements significantly, while the other models under-estimate the measurements. The FI-model, on the other hand, has zero mean errors due to the fact that it is calculated based on minimising the mean errors. The standard deviations of shadow fading in Table 5.1 illustrate that the FI model provides the

minimum error standard deviation and the COST 231-Hata model shows the highest error standard deviation. The FI model shows less standard deviation than the CI model but at the expense of an additional model parameter and lack of physical basis.

Table 5.1: Error statistics of five path-loss models estimations for open area.

	Cost231-Hata	Okumura-Hata	FSPL	CI	FI
μ	-21.4447	5.2337	6.7549	0.8322	0
σ	24.3588	12.68	10.9	9.1	7.68

To compare the measurements with simulation data we used ICS telecom EV software. This software provides the FSPL model and the Okumura-Hata model as empirical path-loss models for 915 MHz. The FSPL model's simulation output is without accounting for the environment diffraction loss and the sub-path loss, while these two factors are considered in the Okumura-Hata model. The recorded data and the estimation of the ICS telecom are shown in Figure 5.3. As Figure 5.3 indicates, the trend of the predicted values using both the FSPL and the Okumura-Hata model are similar in most points. Moreover, it can be observed that both the models are tracking the average value of RSSI values. The error statistics of these path-loss models are presented in Table 5.2.

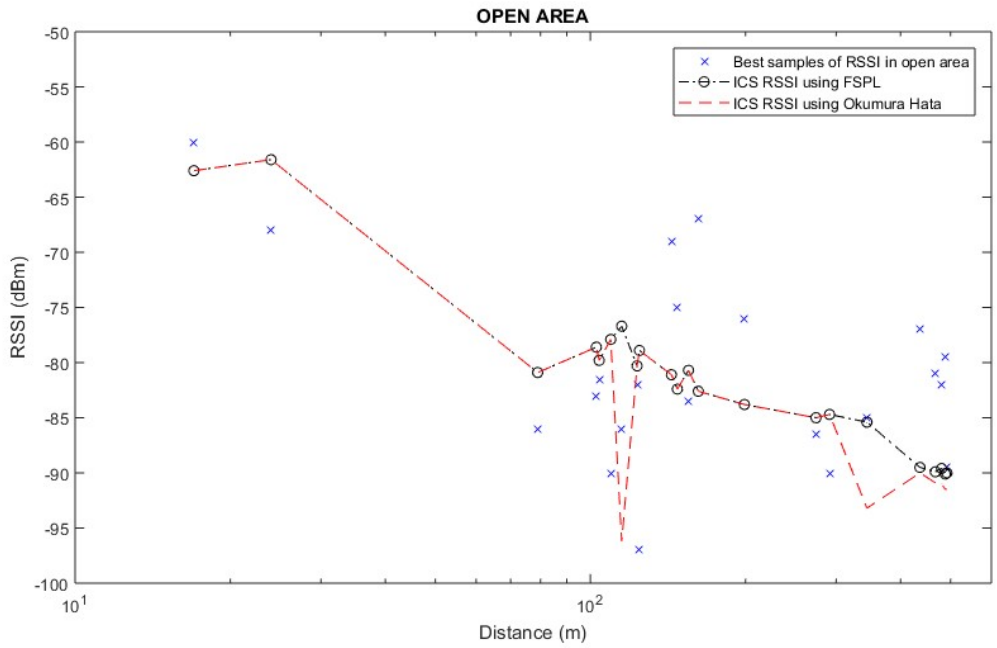

Fig. 5.3: ICS telecom EV estimation for open-area measurements.

Table 5.2: Error statistics of the RSSI generated by using ICS telecom EV for open area.

	Okumura-Hata	FSPL
μ	2.3045	0.8
σ	9	8.55

Table 5.2 shows that the FSPL model performs better than the Okumura-Hata model, which under-predicts the measurements while the FSPL model estimation is very close to the mean value of the measurements. From Tables 5.1 and 5.2, it can be calculated that all the models have rather large standard deviations (7 dB or so). The FI model provides the minimum error, and the standard deviation calculated by the CI model in Table 5.1 is comparable with the standard deviation obtained by ICS telecom. This may encourage users to select a simpler model instead of the one of complicated models.

5.2. Propagation in Rural Area

In the rural area, more than 400 measurements with a time interval of 30 s were recorded at 16 RX locations of the campus for T-R separation distances of up to 750 m. The strongest recorded data in each location is shown in Table B.2 Appendix B. It is noteworthy that the rural measurements were taken in locations where most trees were tall and in full leaf. Consequently, the measurements can be considered to be representative of the worst-case conditions in rural areas.

Similarly to the analysis done for the open-area scenario, the rural measurements were compared with two groups of path-loss models. Figure 5.4 displays the scatter plot and the Okumura-Hata model and the COST 231-Hata model predictions for various T-R separation distances for the rural area. In this figure, both the rural and suburban versions of the Okumura-Hata model are plotted to help us to find the best-fitted model. As Figure 5.4 shows, the rural model of Okumura-Hata under-predicts the measurements, while the COST 231-Hata model and the suburban model of Okumura-Hata over-predict the path loss, but the Okumura-Hata model gives the lower error. Predictions made by the second group, the FSPL model, CI and FI models, are shown in Figure 5.5.

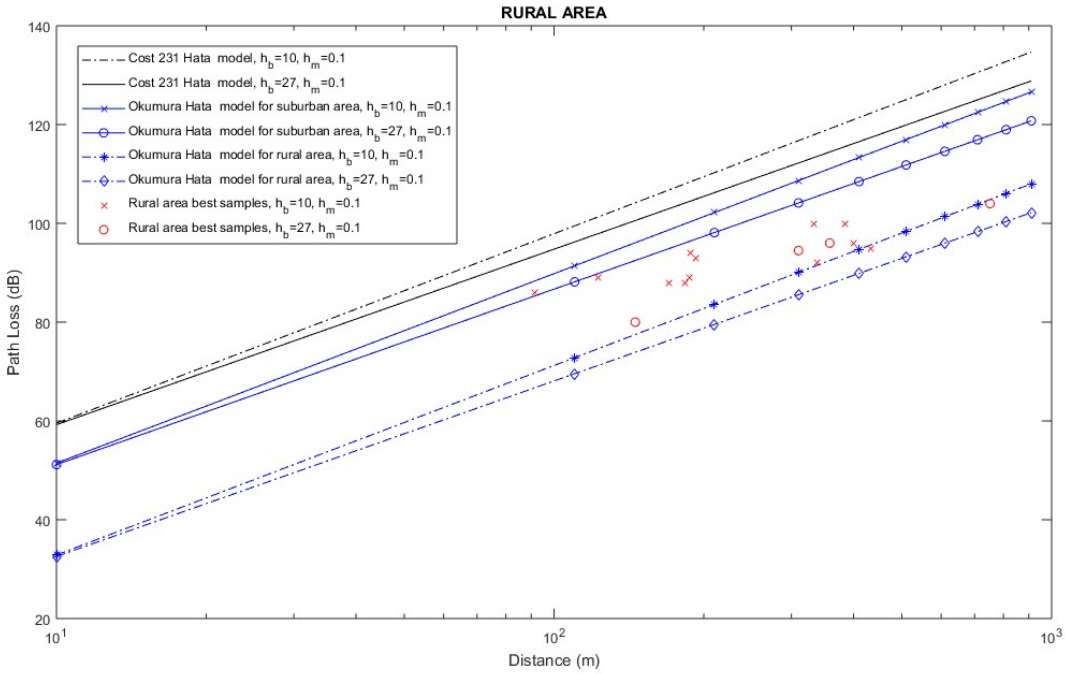

Fig. 5.4: Okumura-Hata model and COST 231-Hata model estimation for rural-area measurements.

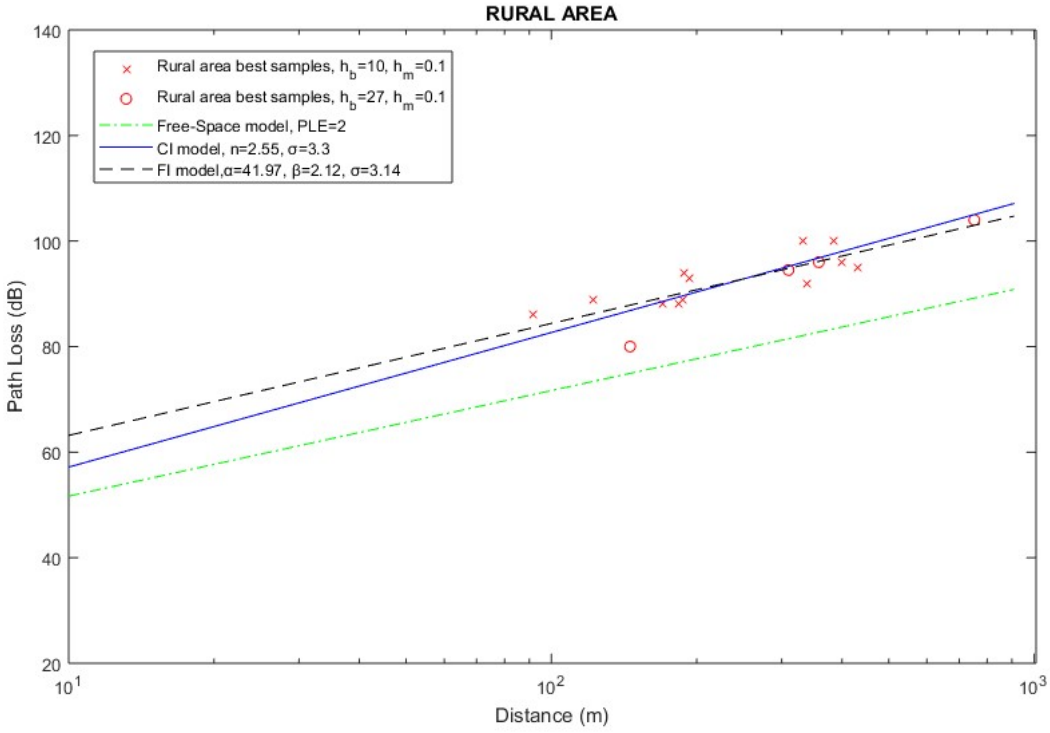

Fig. 5.5: FSPL model, CI model and FI model estimation for rural-area measurements.

The PLE of the CI model is 2.55, greater than what is obtained from open-area measurements, and the parameter β of the FI model increases from 1 in open areas to 2.12 in rural areas, while parameter α decreases from 60.34 to 41.97. As Figure 5.5 shows, the CI and FI models matched the empirical data quite well, whereas the FSPL prediction is significantly lower than the actual value. The error statistics of all the models are presented in Table 5.3.

Table 5.3: Error statistics of five path-loss models' estimations for rural area.

	Cost231-Hata	Okumura-Hata Suburban Model	Okumura-Hata Rural Model	FSPL	CI	FI
μ	-19.1455	-11.0590	7.5328	13.1980	0.0219	0
σ	19.6653	11.9362	8.7701	13.5689	3.3	3.14

From Table 5.3, it is clear that the COST 231-Hata, FSPL and the suburban model of Okumura-Hata estimate errors to be higher than the other models, which means that these models cannot be used to estimate realistic measured path losses in rural areas. On the other hand, the CI and FI models provide the lowest standard deviation and mean of error, and the difference between these two models is not significant, thus motivating the use of the CI model, with fewer parameters.

The ICS telecom outputs, selecting the Okumura-Hata model and the FSPL model as the path-loss models, are presented in Figure 5.6 and the error statistics of the models' estimations are represented in Table 5.4.

Table 5.4: Error statistics of the RSSI generated by using ICS telecom EV for rural area.

	Okumura-Hata	FSPL
μ	1.0813	-6.9250
σ	10.5378	7.7596

As Figure 5.6 and Table 5.4 illustrate, no clear match is observed between the measurements and ICS telecom estimations. Although considering diffraction in the path loss improves the estimation, it is not much. Therefore, both MATLAB and ICS telecom showed that the Okumura-Hata model and the FSPL model are not accurate path-loss models for rural areas.

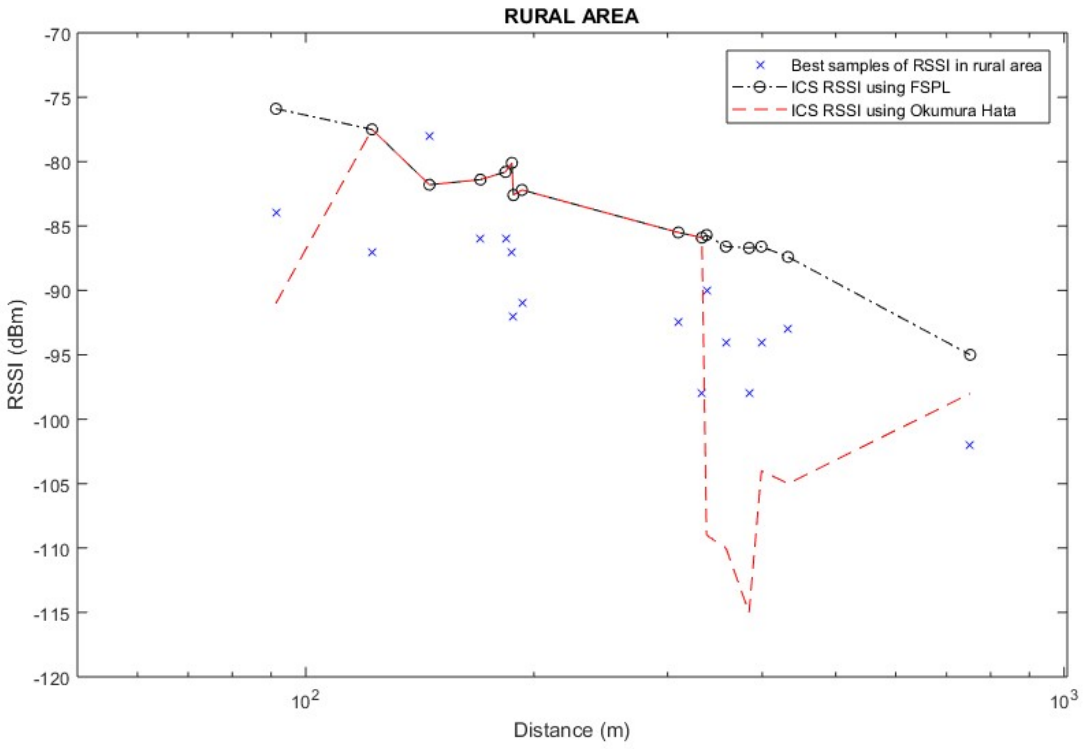

Fig. 5.6: ICS telecom EV estimation for rural-area measurements.

5.3. Propagation in Urban Area

For the urban-area study, 400 measurements in total were recorded at 18 RX locations of the campus with the 3D distance ranging from 20 m to 300 m. Note that, during the measurements, the point G2 was only used for the gateway location. The strongest recorded power at each location is presented in Table B.3 of Appendix B.

Figure 5.7 shows the scatter plot of the measured data in the urban area and the corresponding Okumura-Hata model and the COST 231-Hata model results. In this case, both suburban and urban models are plotted for wider investigation. As Figure 5.7 illustrates, the suburban model of the Okumura-Hata model shows closer agreement with the measurements while the other models predicted a higher path loss.

The recorded data and the CI and FI models are shown in Figure 5.8. Using the MMSE method, the PLE of the CI model is 2.94 and its standard deviation $\sigma = 4.65$ dB, while the FI model provides a standard deviation of $\sigma = 4.57$ dB with $\alpha = 38.71$ and $\beta = 2.62$.

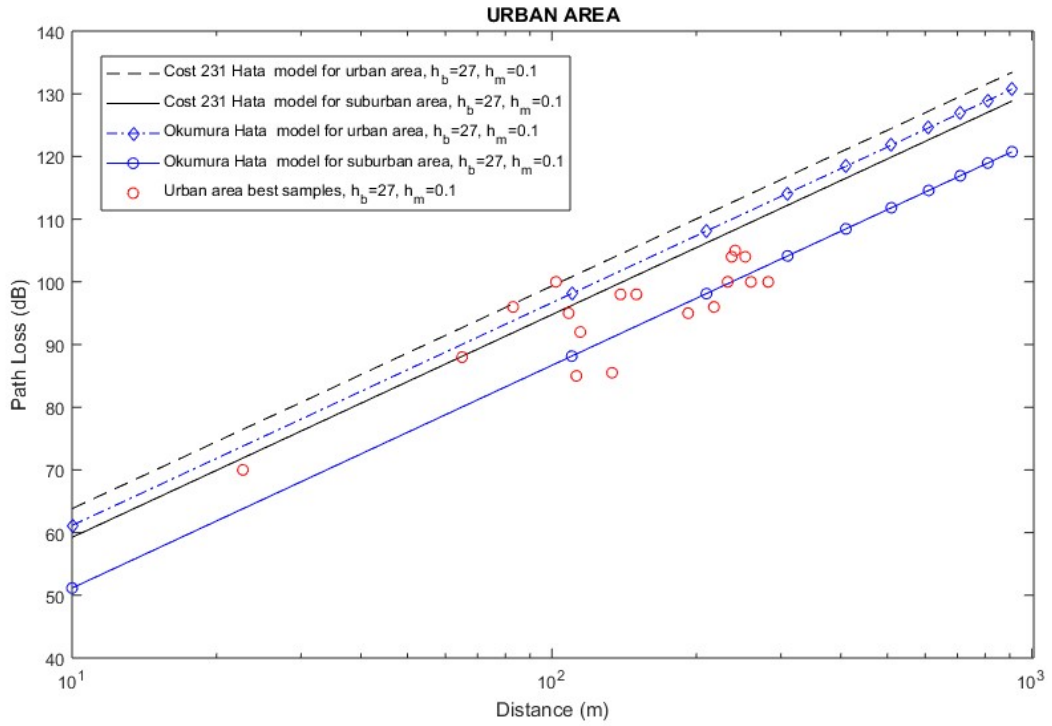

Fig. 5.7: Okumura-Hata model and COST 231-Hata model estimations for urban-area measurements.

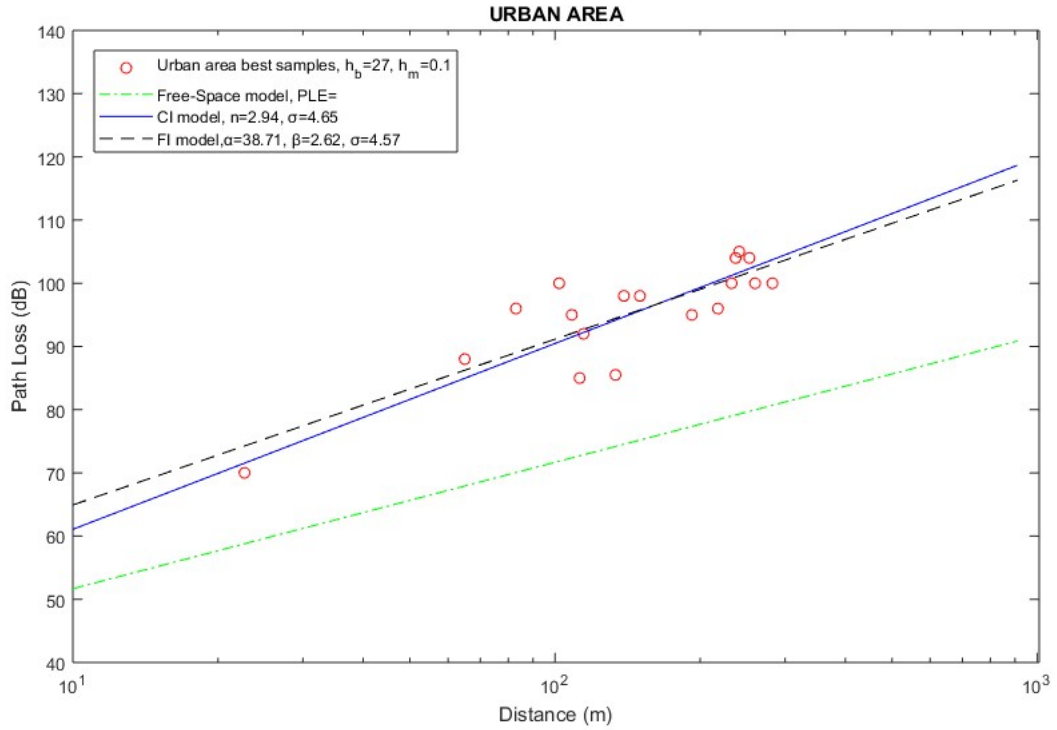

Fig. 5.8: FSPL model, CI model and FI model estimations for urban-area measurements.

The mean error and standard deviation of each model are presented in Table 5.5. The error statistics show a better agreement with the CI and FI models than with the other models. The Okumura-Hata model estimates the measurements better than to the COST 231-Hata model, but the standard deviation of both the models are more than 6 dB, which is high.

Table 5.5: Error statistics of the four path-loss models' estimations for urban area.

	Cost231-Hata Urban Model	Cost231-Hata Suburban Model	Okumura-Hata Urban Model	Okumura-Hata Suburban Model	FSPL	CI	FI
μ	-9.59	-5.01	-6.92	3.07	20.41	0.2	0
σ	10.9	7.22	8.65	6.04	20.98	4.65	4.57

The measurements taken on campus are also used to compare the predictions of the Okumura-Hata model and the FSPL model using ICS telecom. The results are shown in Figure 5.9 and the error statistics prediction of each model are presented in Table 5.6.

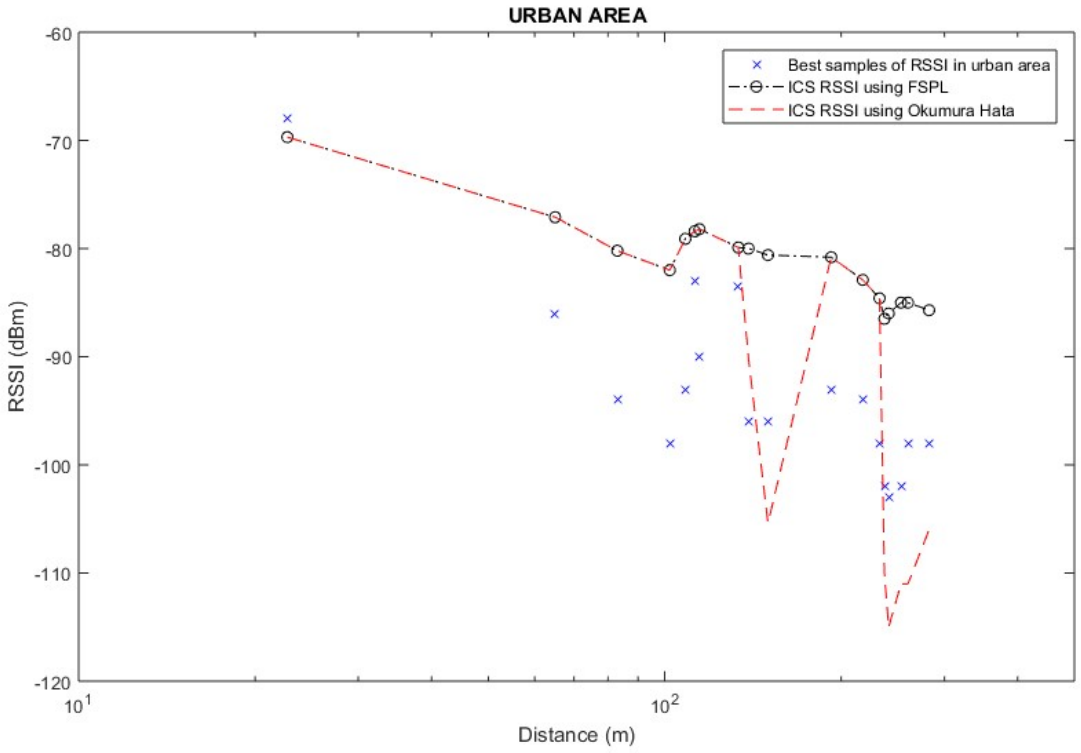

Fig. 5.9: ICS telecom EV estimation for urban area measurements.

From Figure 5.9 and Table 5.6 it is observed that neither model can predict the measurements correctly.

Table 5.6: Error statistics of the RSSI generated by using ICS telecom EV for urban area.

	Okumura-Hata	FSPL
μ	-3	-11.88
σ	10.52	12.86

As discussed before, the error statistics of all the path-loss models show that, by definition, the CI and FI models are better fitted to the measurements. The parameters of these two models are summarised in Table 5.7 based on the environment types.

The PLE of the CI model in Table 5.7 shows that the path loss is much greater in rural areas than in open areas, and the urban-area propagation is higher than in rural areas, likely due to increased scattering, diffraction and reflection. The parameter α of FI model decreases while parameter β increase with increasing the obstacles between the transmitter and receiver antennas. Moreover, The FI model parameters variation is wider than the CI model parameter's. Moreover, the shadow-fading factor of the both the CI model and the FI model is decreased with increasing the environment obstacles. It is also clear that, although the CI model provides a slightly higher shadow-fading standard deviation than the FI model, this difference is not significant. As there is a little value in using a model with more than one parameter, and the CI model offers a parameter that make sense physically, it can be concluded that the single-parameter CI model is a more appropriate option for modelling the path loss in T-R communication.

Table 5.7: Path-loss parameters of CI and FI models for various environment types.

	CI Model		FI Model		
	n	σ	α	β	σ
Open area	2.27	9.1	60.34	1	7.68
Rural area	2.55	3.3	41.97	2.12	3.14
Urban area	2.94	4.65	38.71	2.62	4.54

5.4. LoRa Coverage Area

In a wireless network, the reliability of transmission is very important. It is essential for users to know how much of an area is effectively covered by a base station, or a heavy signal loss due to harsh environmental conditions will result unreliable information transmission.

Based on Table 2.2, a LoRa receiver is able to recognise signals with an RSSI above -137 dBm by using SF12 and a BW of 125 kHz. A critical question here is whether signals with power -137 dBm are able to provide a reliable result in the ThingSpeak channels. To address this question, we randomly distributed a number of temperature sensors over an area of 1.5 km (Figure 5.10). The measured temperature and the RSSI of each location were transmitted to the ThingSpeak channels every 10 minutes via the LoRa network described in Section 4.3.3. The experiment was conducted during the night from 7 pm to 7 am to have the least diffraction from moving people and vehicles. Analysis of the data stored in the channels enables us to determine what percentage of the area will be covered by the LG01-S according to the propagation characteristics of the environment, and what power level defines the edge of this area.

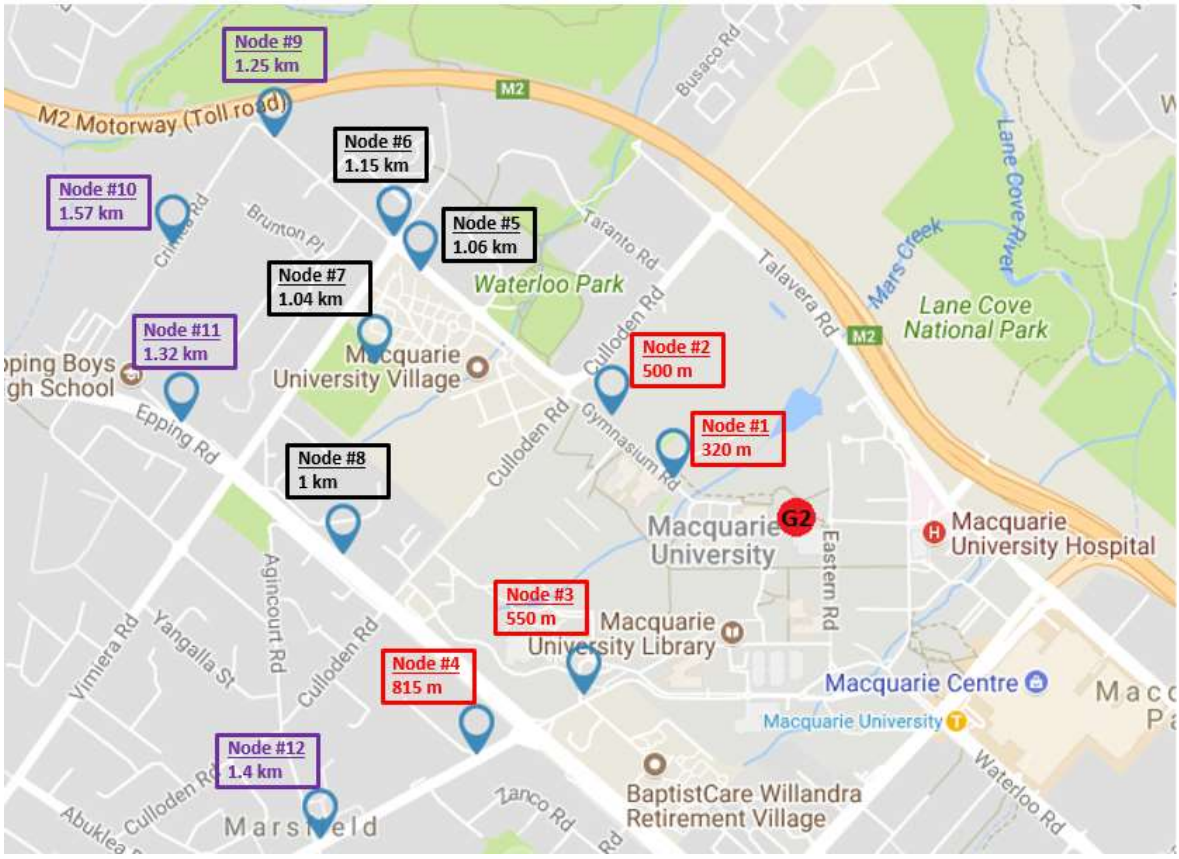

Fig. 5.10: LoRa nodes within a radius of 1.5 km.

As a maximum of eight variables can be shown in each channel, we divided the nodes into three groups based on the distance from the gateway. Group 1: Node 1 to Node 4, Group2: Node 5 to Node 8; Group 3: Node 9 to Node 12.

Figure 5.11 shows that the data captured from Group 1, with a maximum distance of 815 m from the gateway. As Figure 5.11 shows, the RSSI value in the Node1 location fluctuates between -98 dBm and -97 dBm, but the strongest value is -97 dBm. With increasing distance RSSI decreases to -100 dBm in Node 2 and Node 3, and RSSI in Node 4 varies between -102 dBm and -101 dBm very quickly. The fast fluctuation in RSSI from Nodes 1, 2 and 4 is the effect of the tall obstacles between the LG01 and the nodes. Figure 5.11 also shows that the Node 1 to Node 4 outputs are regular and periodic.

The outputs of Group 2 are shown in Figure 5.12; the minimum distance from the gateway in this case is 1 km and the maximum distance is 1.15 km. Figure 5.12 shows that the received data is periodic as long as the average value of RSSI is higher than -100 dBm, and the quality of the received signal will decrease when the average value of RSSI reaches below -100 dBm. If the RSSI value of the signal goes less than -100 dBm, then that means some packets of data have been lost during the transmission period. In addition, no data have been received from the nodes for a long time by the ThingSpeak channel. For example, no signal has been received from Node 6 for four hours (from 10 pm to 2 am). This shows that LG01 cannot cover that location properly.

In this experiment no signal was received at the ThingSpeak channels from Group 3, which were more than 1.2 km away from the gateway. So, this experiment shows that the best coverage area of the LG01-S is around 1 km with the threshold power of -100 dBm.

Fig. 5.11: Received data from Node 1 to Node 4 in ThingSpeak.

Fig. 5.12: Received data from Node 5 to Node 8 in ThingSpeak.

To investigate which path-loss model better predicts the coverage area, we selected a group of nodes (Node 1, Node 2, Node 5 and Node 6) located in different environment types. The nodes' distribution based on distance and environment type are as follows:

Distance range	Environment type	Node
$0\ \text{m} < d \leq 250\ \text{m}$	Open area	-
$250\ \text{m} < d \leq 900\ \text{m}$	Rural area	Node 1, Node 2
$900\ \text{m} < d \leq 1.5\ \text{km}$	Urban area	Node 5, Node 6

The measured RSSI and the estimations of the CI model and the FI model are presented in Figure 5.13. As Figure 5.13 shows, the CI model prediction for the received signal power and coverage area is close to what was obtained from the experiment, while the FI model over-predicts both the received signal power and the coverage area. Therefore, this research shows that the CI model estimates the coverage area better than the FI model.

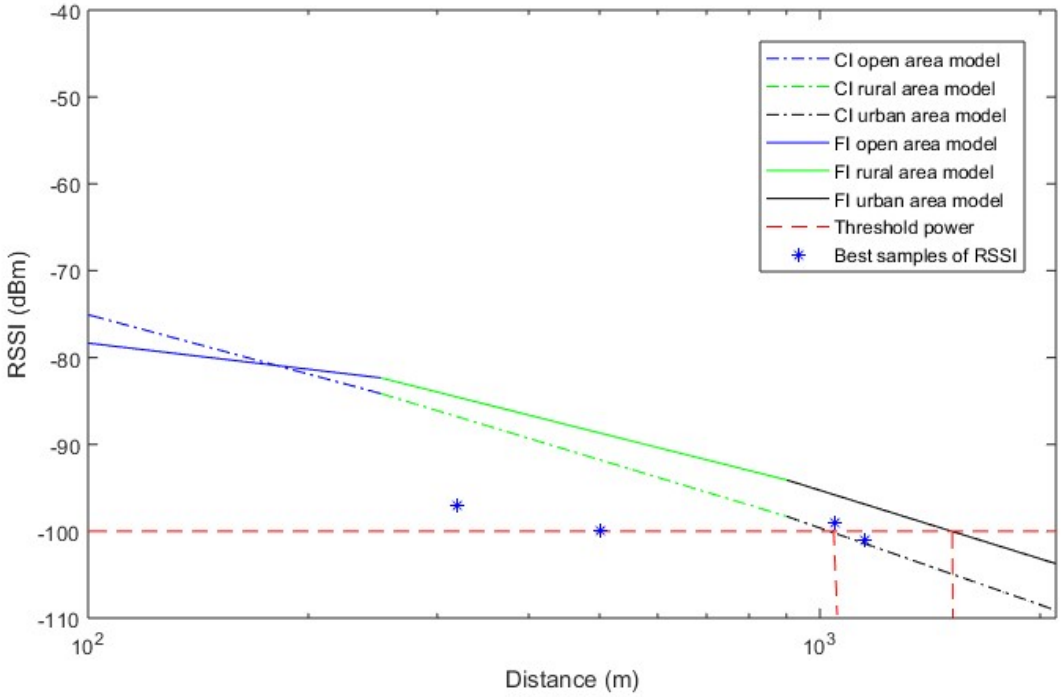

Fig. 5.13: Coverage area estimation using CIand FI path-loss models.

5.5. Chapter Summary

In this chapter, measurements taken in open, rural and urban areas of the University campus are compared with the estimations of the FSPL, Okumura-Hata and COST 231-Hata models. Also, the CI and FI path-loss model for each scenario was calculated by using the MMSE method, and all the path-loss models were compared in terms of error standard deviations. This chapter shows that the FI model is the best-fitted path-loss model for each scenario, but is very sensitive to the geographical environment and the number of measurements. The predictions of the CI model for the coverage area and signal propagation outside the test environments are more accurate than those from the FI model.

Chapter 6
Conclusions and Future Works

This research studied the performance of LoRa technology as a long-range IoT in different environments. The important findings from this investigation are pointed out in this chapter, which also outlines the recommended directions for future research.

6.1. Conclusions

This project has presented path-loss models based on measurements taken in three environment types of the Macquarie University campus: open area, rural area and urban area. The empirical measurements were analysed against two groups of empirical path-loss models: 1) the models which are commonly used in the ISM band, namely the COST 231-Hata, the Okumura-Hata model and the FSPL model, and 2) the physically based path-loss models calculated by minimising the model's standard deviation via the MMSE approach, namely the CI and FI models.

Signal-propagation analysis shows that the COST 231-Hata model generally over-predicts the propagation loss in most cases. This is perhaps to be expected owing to the fact that it is more suitable for mobile radio planning. We found that the Okumura-Hata model in general under-estimates the path loss, especially at greater antenna height. Besides, it shows that the Okumura-Hata open-area model is best fitted to open- and rural-areas measurements while the suburban model better describes the path loss for urban-area measurements. We also found that the LOS measurement data are closely modelled by the FSPL model, while the NLOS measurement data are not accurately estimated by the FSPL model.

The experiment analysis shows that the FI path-loss model, as a two-parameter model, provides the lowest standard deviation in a majority of scenarios compared to other propagation models. It is also shown that the FI model is very sensitive to the geogeraphical environment and the number of measurements, and the slope variation of this model is between 1 and 2.62 for LOS and NLOS scenarios.

The CI model is another fitted path-loss model which accurately predicts signal propagation using just one parameter. The CI model is frequency-dependent and the parameter *n* or PLE represents the environment's effects on path loss. Using the MMSE method, the CI path-loss model resulted in a PLE of nearly 2.27, 2.55 and 2.94 for open, rural and urban areas, respectively. This shows that the stability of the CI model parameter is higher than that of the parameters of the FI model. The extensive experiments also showed that the CI model has a better prediction ability in terms of standard deviation for a variety of different distances and environments that are different from those used for determining the CI model parameter originally. It was also shown that the prediction of the CI model for the coverage area with a threshold power of -100 dBm is much more accurate than for the FI model. Therefore, for the estimation of signal propagation and LoRa coverage area outside the test environments used for the model, this project suggests that the CI model is more robust and reliable than the other path-loss models.

6.2. Future Works

The research presented in this thesis has provided answers to several critical questions regarding the performance of LoRa. However, there is a lot more research to be conducted to get a complete picture. The following topics are recommended as the future avenues of research:

- In our project, limited end-devices were reporting their data in the network, while in a real network there may be thousands of end-devices in a single cell. In such a scenario, we are faced with several challenges. Firstly, an increase in transmitter power consumption as the transmitters will have to resend packets several times due to collisions, which will affect the battery life. Secondly, data collision on the receiver side will increase the probability of packet errors. Choosing the right values for parameters such as SF, BW can alleviate these problems.
- Use of acknowledge (ACK) messages increases the reliability of communication between the transmitter and receiver. However, this also increases the overhead and therefore the traffic. Reduction in the use of ACK messages means supporting more end nodes. Since

LoRa aims to support a million devices in a network, exploring this trade-off between the use of ACK vs a higher number of devices can play an important role.

- Although the results derived in our work provide a good insight into the coverage performance of LoRa, we were limited by the physical constraints imposed by a university campus. It will be interesting to see the effect of the parameters such as SF, BW and CR in determining the coverage area over different environments.
- Use of different classes of LoRa (A, B, C) influence on the traffic of a network. It would be interesting to investigate the effect of each class on the size of a LoRa network.
- There are other technologies available as part of LPWAN, e.g. SIGFOX, NB-IoT, EC-GSM and LTE-M. Study of these technologies and the comparison are also important.

Appendices

Here mathematical methods for minimising the standard deviation of the CI and FI models are presented in Appendix A. Moreover, the raw data used to obtain the path-loss models are given in Appendix B and the code written in this project is provided in Appendix C.

Appendix A

CI path-loss model:

The shadow fading (SF) of the single-frequency close-in (CI) model, which is defined in (3.7), is as follows [67]:

$$X_{\sigma}^{\mathrm{CI}} = \mathrm{PL}^{\mathrm{CI}}(f,d)[\mathrm{dB}] - 20\log_{10}\left(\frac{4\pi f_c}{c}\right) - 10n\log_{10}(d) = A - nD \tag{A.1}$$

where A is $\mathrm{PL}^{\mathrm{CI}}(f,d)[\mathrm{dB}] - 20\log_{10}\left(\frac{4\pi f_c}{c}\right)$ and D represents $10n\log_{10}(d)$. It follows that the standard deviation of the random variable X_{σ}^{CI} is

$$\sigma^{\mathrm{CI}} = \sqrt{\sum {X_{\sigma}^{\mathrm{CI}}}^2/N} = \sqrt{\sum (A-nD)^2/N} \tag{A.2}$$

where N is the number of measured data. Minimising σ^{CI} is equivalent to minimising the term $\sum(A-nD)^2$. To minimize $\sum(A-nD)^2$, the derivative with respect to n should be zero:

$$\frac{d\sum(A-nD)^2}{dn} = \sum 2D(nD-A) = 2\sum D(nD-A) = 2\left(n\sum D^2 - \sum DA\right) = 0 \tag{A.3}$$

Therefore

$$n = \frac{\sum DA}{\sum D^2} \tag{A.4}$$

so the minimum standard deviation for the CI model is

$$\sigma_{min}^{\mathrm{CI}} = \sqrt{\sum (A - D\frac{\sum DA}{\sum D^2})^2 / N} \tag{A.5}$$

If A and D are written as column vectors, n can be expressed in matrix form as

$$n = A^T (D^T D)^{-1} D \tag{A.6}$$

and hence the minimum standard deviation for the CI model becomes

$$\sigma_{min}^{\mathrm{CI}} = \sqrt{\sum (A - (A^T (D^T D)^{-1} D) D)^2 / N} \tag{A.7}$$

FI path-loss model:

The SF of the floating-intercept (FI) model, which is defined by (3.8), is given as follows:

$$X_\sigma^{\mathrm{FI}} = B - \alpha - \beta D \tag{A.8}$$

and the standard deviation for the model is:

$$\sigma^{\mathrm{FI}} = \sqrt{\sum {X_\sigma^{\mathrm{FI}}}^2 / N} = \sqrt{\sum (B - \alpha - \beta D)^2 / N} \tag{A.9}$$

The term $\sum (B - \alpha - \beta D)^2$ is to be minimised in order to minimise σ^{FI}, which means that its partial derivatives with respect to α and β should be zero, such that:

$$\frac{\partial \sum (B - \alpha - \beta D)^2}{\partial \alpha} = \sum 2(\alpha + \beta D - B) = 2\left(N\alpha + \beta \sum D - \sum B\right) = 0 \tag{A.10}$$

$$\frac{\partial \sum (B - \alpha - \beta D)^2}{\partial \beta} = \sum 2D(\alpha + \beta D - B) = 2\left(\alpha \sum D + \beta \sum D^2 - \sum DB\right) = 0 \tag{A.11}$$

Combining (A.10) and (A.11) yields:

$$\alpha = \frac{\sum D \sum DB - \sum D^2 \sum B}{(\sum D)^2 - N \sum D^2} \tag{A.12}$$

$$\beta = \frac{\sum D \sum B - N \sum DB}{(\sum D)^2 - N \sum D^2} \tag{A.13}$$

and α and β can be expressed in matrix form as:

$$\beta = (D - \bar{D})^T \left((D - \bar{D})^T (D - \bar{D})\right)^{-1} (B - \bar{B}) \tag{A.14}$$

$$\alpha = \bar{B} - \beta \bar{D} \tag{A.15}$$

where $\bar{D}$ and $\bar{B}$ denote the mean values of the elements in matrix D and B, respectively.

Appendix B

Table B.1: The strongest value of the recorded RSSI in open area

Gateway Location			Node Location		Measured Data in Open Area	
Latitude	Longitude	h_b (m)	Latitude	Longitude	Distance (m)	RSSI (dBm)
-33.773023	151.113557	10	-33.773	151.1136	17	-60
			-33.772	151.1136	79	-86
			-33.772	151.114	123.2	-82
			-33.772	151.1141	104	-81.5
			-33.772	151.1143	109.5	-90
			-33.772	151.1144	155	-83.5
			-33.772	151.1138	147.5	-75
			-33.773	151.1147	115	-86
			-33.772	151.1128	102.7	-83
			-33.773	151.1124	124.5	-97
			-33.771	151.1147	291.2	-90
			-33.77	151.1156	344.1	-85
-33.774401	151.11467	27	-33.775	151.1135	143.6	-69
			-33.776	151.1138	162	-67
			-33.771	151.1113	480.4	-82
			-33.771	151.1115	491.9	-89.5
			-33.771	151.1117	488.4	-79.5
			-33.771	151.1118	467.2	-81
			-33.771	151.1119	436.1	-77
			-33.774	151.1145	24	-68
			-33.773	151.116	199	-76
			-33.772	151.1166	274	-86.5

Table B.2: The strongest value of the recorded RSSI in rural area

Gateway Location			Node location		Measured Data in Rural Area	
Latitude	Longitude	h_b (m)	Latitude	Longitude	Distance (m)	RSSI (dBm)
-33.773023	151.113557	10	-33.772494	151.114313	91.36	-84
			-33.77231	151.114565	122.3	-87
			-33.769983	151.115532	384.3	-98
			-33.770332	151.115251	337.7	-90
			-33.771365	151.112947	192.8	-91
			-33.772548	151.111617	187	-87
			-33.771195	151.109842	399	-94
			-33.770367	151.110138	432.6	-93
			-33.770268	151.112149	333	-98
			-33.771362	151.113187	187.9	-92
			-33.771569	151.112988	170	-86
			-33.771814	151.112207	183.4	-86
-33.774401	151.11467	27	-33.774442	151.113095	145.6	-78
			-33.774365	151.111317	310	-92.5
			-33.774306	151.110797	358.2	-94
			-33.767634	151.113017	752.7	-102

Table B.3: The strongest value of the recorded RSSI in urban area

Gateway Location			Node location		Measured Data in Urban Area	
Latitude	Longitude	h_b (m)	Latitude	Longitude	Distance (m)	RSSI (dBm)
-33.774401	151.11467	27	-33.774951	151.113104	22.7	-68
			-33.774733	151.112733	65	-86
			-33.774493	151.112036	133.5	-83.5
			-33.772948	151.112699	237	-102
			-33.773263	151.1144	217.7	-94
			-33.774277	151.114164	112.5	-83
			-33.774404	151.115288	192.3	-93
			-33.775284	151.114924	150	-96
			-33.775767	151.114079	108.4	-93
			-33.776417	151.115193	232.5	-98
			-33.776111	151.116093	282.5	-98
			-33.774173	151.110795	253	-102
			-33.774928	151.112104	114.6	-90
			-33.774940	151.113655	102	-98
			-33.774154	151.115811	139	-96
			-33.775233	151.111776	260	-98
			-33.773113	151.116558	241	-103
			-33.774477	151.115429	83	-94

Appendix C

Part 1

- **LoRa client code**

```
/*
  LoRa Simple Client for Arduino :
  Support Devices: LoRa Shield + Arduino

*/

#include <SPI.h>
#include <RH_RF95.h>

// Singleton instance of the radio driver
RH_RF95 rf95;
float frequency = 915.0;

void setup()
{
  Serial.begin(9600);
  while (!Serial) ; // Wait for serial port to be available
  Serial.println("Start LoRa Client");
  if (!rf95.init())
    Serial.println("init failed");
  // Setup ISM frequency
  rf95.setFrequency(frequency);
  // Setup Power,dBm
  rf95.setTxPower(20);
  rf95.setSpreadingFactor(12);
  // rf95.setSignalBandwidth(500000);
  //rf95.setCodingRate4(8);
  // Defaults after init are 434.0MHz, 13dBm, Bw = 125 kHz, Cr = 4/5, Sf = 128chips/symbol, CRC on
}

void loop()
{
  Serial.println("Sending to LoRa Server");
  // Send a message to LoRa Server
  uint8_t data[] = "Hello World!";
  rf95.send(data, sizeof(data));

  rf95.waitPacketSent();
  // Now wait for a reply
  uint8_t buf[RH_RF95_MAX_MESSAGE_LEN];
  uint8_t len = sizeof(buf);

  if (rf95.waitAvailableTimeout(3000))
  {
    // Should be a reply message for us now
    if (rf95.recv(buf, &len))
    {
      Serial.print("got reply: ");
      Serial.println((char*)buf);
      Serial.print("RSSI: ");
      Serial.println(rf95.lastRssi(), DEC);
```

```
    }
    else
    {
      Serial.println("recv failed");
    }
  }
  else
  {
    Serial.println("No reply, is LoRa server running?");
  }
  delay(5000);
```

- **LoRa server code**

```
/*
  LoRa Simple Yun Server :
  Support Devices: LG01.
*/
//If you use Dragino IoT Mesh Firmware, uncomment below lines.
//For product: LG01.
#define BAUDRATE 115200

//If you use Dragino Yun Mesh Firmware , uncomment below lines.
//#define BAUDRATE 250000

#include <Console.h>
#include <SPI.h>
#include <RH_RF95.h>

// Singleton instance of the radio driver
RH_RF95 rf95;

int led = A2;
float frequency = 915.0;

void setup()
{
  pinMode(led, OUTPUT);
  Bridge.begin(BAUDRATE);
  Console.begin();
  while (!Console) ; // Wait for console port to be available
  Console.println("Start Sketch");
  if (!rf95.init())
    Console.println("init failed");
  // Setup ISM frequency
  rf95.setFrequency(frequency);
  // Setup Power,dBm
  rf95.setTxPower(20);
  rf95.setSpreadingFactor(12);
  // Defaults BW Bw = 125 kHz, Cr = 4/5, Sf = 128chips/symbol, CRC on
  Console.print("Listening on frequency: ");
  Console.println(frequency);
}

void loop()
{
  if (rf95.available())
  {
```

```
    // Should be a message for us now
    uint8_t buf[RH_RF95_MAX_MESSAGE_LEN];
    uint8_t len = sizeof(buf);
    if (rf95.recv(buf, &len))
    {
     digitalWrite(led, HIGH);
     RH_RF95::printBuffer("request: ", buf, len);
     Console.print("got request: ");
     Console.println((char*)buf);
     Console.print("RSSI: ");
     Console.println(rf95.lastRssi(), DEC);

     // Send a reply
     uint8_t data[] = "And hello back to you";
     rf95.send(data, sizeof(data));
     rf95.waitPacketSent();
     Console.println("Sent a reply");
     digitalWrite(led, LOW);
    }
    else
    {
     Serial.println("recv failed");
    }
   }
}
```

Part 2

- **LoRa client code**

```
/*
  Upload Data to IoT Server ThingSpeak (https://thingspeak.com/):
  Support Devices: LoRa Shield + Arduino

  Example sketch showing how to read Temperature and Humidity from DHT11 sensor,
  Then send the value to LoRa Server, the LoRa Server will send the value to the
  IoT server
The code for other nodes are the same it is only necessary to change the node ID

*/

#include <SPI.h>
#include <RH_RF95.h>
#include <String.h>

RH_RF95 rf95;

#define dht_dpin A0 // Use A0 pin as Data pin for DHT11.
byte bGlobalErr;
char dht_dat[5]; // Store Sensor Data
String stringOne;
float frequency = 915.0;

void setup()
{
   InitDHT();
   Serial.begin(9600);
```

```
  if (!rf95.init())
    Serial.println("init failed");
  // Setup ISM frequency
  rf95.setFrequency(frequency);
  // Setup Power,dBm
  rf95.setTxPower(20);
  rf95.setSpreadingFactor(12);

  Serial.println("Humidity and temperature\n\n");
}

void InitDHT()
{
  pinMode(dht_dpin,OUTPUT);//Set A0 to output
  digitalWrite(dht_dpin,HIGH);//Pull high A0
}

//Get Sensor Data
void ReadDHT()
{
  bGlobalErr=0;
  byte dht_in;
  byte i;

  //pinMode(dht_dpin,OUTPUT);
  digitalWrite(dht_dpin,LOW);//Pull Low A0 and send signal
  delay(30);//Delay > 18ms so DHT11 can get the start signal

  digitalWrite(dht_dpin,HIGH);
  delayMicroseconds(40);//Check the high level time to see if the data is 0 or 1
  pinMode(dht_dpin,INPUT);
  // delayMicroseconds(40);
  dht_in=digitalRead(dht_dpin);//Get A0 Status
  //  Serial.println(dht_in,DEC);
  if(dht_in){
    bGlobalErr=1;
    return;
  }
  delayMicroseconds(80);//DHT11 send response, pull low A0 80us
  dht_in=digitalRead(dht_dpin);

  if(!dht_in){
    bGlobalErr=2;
    return;
  }
  delayMicroseconds(80);//DHT11 send response, pull low A0 80us
  for (i=0; i<5; i++)//Get sensor data
  dht_dat[i] = read_dht_dat();
  pinMode(dht_dpin,OUTPUT);
  digitalWrite(dht_dpin,HIGH);//release signal and wait for next signal
  byte dht_check_sum = dht_dat[0]+dht_dat[1]+dht_dat[2]+dht_dat[3];//calculate check sum
  if(dht_dat[4]!= dht_check_sum)//check sum mismatch
    {bGlobalErr=3;}
};

byte read_dht_dat(){
  byte i = 0;
  byte result=0;
```

```
  for(i=0; i< 8; i++)
  {
    while(digitalRead(dht_dpin)==LOW);//wait 50us
    delayMicroseconds(30);//Check the high level time to see if the data is 0 or 1
    if (digitalRead(dht_dpin)==HIGH)
    result |=(1<<(7-i));//
    while (digitalRead(dht_dpin)==HIGH);//Get High, Wait for next data sampleing.
  }
  return result;
}


void loop()
{

uint8_t buf[RH_RF95_MAX_MESSAGE_LEN];//Reply data array
  uint8_t len = sizeof(buf);//reply data length

  if (rf95.waitAvailableTimeout(3000))// Check If there is reply in 3 seconds.
  {
    // Should be a reply message for us now
    if (rf95.recv(buf, &len))//check if reply message is correct
    {
       if(buf[0] == 1||buf[1] == 1||buf[2] ==1) // Check if reply message has the our node ID
       {
          Serial.print("got reply: ");//print reply
          Serial.println((char*)buf);
          Serial.print("RSSI: ");  // print RSSI
          Serial.println(rf95.lastRssi(), DEC);
          ReadDHT();
  char data[50] = {0} ;
  // Use data[0], data[1],data[2] as Node ID
  data[0] = 1 ;
  data[1] = 1 ;
  data[2] = 1 ;
  data[3] = dht_dat[0];//Get Humidity
  data[4] = dht_dat[2];//Get Temperature
  switch (bGlobalErr)
  {
   case 0:
      Serial.print("Current humdity = ");
      Serial.print(data[3], DEC);//Show humidity
      Serial.print(".");
      Serial.print(dht_dat[1], DEC);//Show humidity
      Serial.print("%  ");
      Serial.print("temperature = ");
      Serial.print(data[4], DEC);//Show temperature
      Serial.print(".");
      Serial.print(dht_dat[3], DEC);//Show temperature
      Serial.println("C  ");
      break;
    case 1:
      Serial.println("Error 1: DHT start condition 1 not met.");
      break;
    case 2:
      Serial.println("Error 2: DHT start condition 2 not met.");
      break;
    case 3:
```

```
        Serial.println("Error 3: DHT checksum error.");
        break;
      default:
        Serial.println("Error: Unrecognized code encountered.");
        break;
    }

    unsigned char sendBuf[50]=[25];
    int i;

    for(i = 0;i < 5;i++)
    {
       sendBuf[i] = data[i] ;
    }

    sendBuf[5] = rf95.lastRssi() ;

          rf95.send(sendBuf, strlen((char*)sendBuf));//Send LoRa Data

         }
       }
       else
    {
       Serial.println("No reply, is rf95_server running?");//No signal reply

    }

    }

    delay(60000); // Send sensor data every 30 seconds
}
```

- **LoRa server code**

```
/*
  Upload Data to IoT Server ThingSpeak (https://thingspeak.com/):
  Support Devices: LG01

  Example sketch showing how to get data from remote LoRa node,
  Then send the value to IoT Server
*/

#include <SPI.h>
#include <RH_RF95.h>
#include <Console.h>
#include "ThingSpeak.h"
#include "YunClient.h"
YunClient client;
RH_RF95 rf95;

//If you use Dragino IoT Mesh Firmware, uncomment below lines.
//For product: LG01.
#define BAUDRATE 115200

uint16_t crcdata = 0;
uint16_t recCRCData = 0;
float frequency = 915.0;
```

```
void setup()
{
   Bridge.begin(BAUDRATE);
//    Console.begin();// Don't use Console here, since it is conflict with the ThinkSpeak library.

   ThingSpeak.begin(client);

   if (!rf95.init())
      //Console.println("init failed");
   ;
   // Setup ISM frequency
   rf95.setFrequency(frequency);
   // Setup Power,dBm
   rf95.setTxPower(20);
    rf95.setSpreadingFactor(12);
   //Console.println("Start Listening ");
}

void loop()
{

for (int jj = 1; jj < 4; jj++)
{
   uint8_t data[] = "   send data";//Reply
   data[0] = jj;
   data[1] = jj;
   data[2] = jj;
    rf95.send(data, sizeof(data));// Send Request to LoRa Node
    rf95.waitPacketSent();
   if (rf95.waitAvailableTimeout(2000))// Listen Data from LoRa Node
   {
      uint8_t buf[RH_RF95_MAX_MESSAGE_LEN];//receive data buffer
      uint8_t len = sizeof(buf);//data buffer length
      if (rf95.recv(buf, &len))//Check if there is incoming data
      {
            if(buf[0] == jj || buf[1] == jj || buf[2] == jj) //Check if the ID match the LoRa Node ID

            {

               int newD[4] = {0, 0, 0, 0}; //Store Sensor Data here
               for (int i = 0; i < 2; i++)
               {
                  newD[i] = buf[i + 3];
               }
               newD[2] = buf[5];
               int h = newD[0];
               int t = newD[1];
               int rs = newD[2]-256;

               int newData = rf95.lastRssi();

               unsigned long myChannelNumber = 433054;
               const char * myWriteAPIKey = "83E4YB4CYLD7ZMZC";

               if( jj== 1)
               {
               ThingSpeak.setField(1,t);
               ThingSpeak.setField(2,rs);
```

```
            }

              if( jj== 2)
              {
              ThingSpeak.setField(3,t);
              ThingSpeak.setField(4,rs);
              }

              if( jj== 3)
              {
              ThingSpeak.setField(5,t);
              ThingSpeak.setField(6,rs);
              }

              ThingSpeak.writeFields(myChannelNumber, myWriteAPIKey);   // Send Data to IoT Server.
            }
          }
        }
         delay(200000);
    }
}
```

Part 3

```
function [ pl ] = hata_model (fc,hb, hm)
%f in MHz

dmeter=10:100:1e+3;
d=dmeter/1000;
Lent=length(d);
for j=1:length(hb)
   for z=1:length(hm)
      for i=1:length(d)

       ahm(i) = 3.2*(log10(11.75*hm(z))).^2 - 4.97;%large City & fc>400MHz
%      ahm(i)=(1.1*log10(fc)-0.7)*hm(z)-(1.56*log10(fc)-0.8);%smal and medium city

      L50urban1(i) = 69.55 + 26.16*log10(fc) + (44.9 - 6.55*log10(hb(j)))*log10(d(i)) - 13.82*log10(hb(j)) - ahm(i);
      L50suburban1(i) = L50urban1(i) - 2*(log10(fc/28)).^2 - 5.4;
      L50rural1(i) = L50urban1(i) - 4.78*(log10(fc)).^2 + 18.33*log10(fc) - 40.94;
      end
      pl=L50urban1;
%     pl=L50suburban1;
 %    pl=L50rural1;
      semilogx(dmeter, pl, '-.Dg')
   end
end
end
```

Part 4

```
function [ pl ] = cost231hata( fc,hb,hm )
%f in MHz

dmeter=10:100:1e+3;
d=dmeter/1000;
Lent=length(d);
for j=1:length(hb)
   for z=1:length(hm)
```

```
      for i=1:length(d)
         cm_r=0;%rural &suburb
         ahm_r=(1.11.*log10(fc)-0.7)*hm(z)-(1.5.*log10(fc)-0.8);%rural &suburb
         PLch_r(i)=46.3+33.9*log10(fc)-13.82*log10(hb(j))-ahm_r+(44.9-6.55*log10(hb(j)))*log10(d(i))+cm_r;
         cm_u=3;%urban
         ahm_u=3.20.*(log10(11.75*hm(z))).^2-4.97;%urban
         PLch_u(i)=46.3+33.9*log10(fc)-13.82*log10(hb(j))-ahm_u+(44.9-6.55*log10(hb(j)))*log10(d(i))+cm_u;
      end
      pl=PLch_r;
%     pl=PLch_u;
      semilogx(dmeter, pl, '-.r')
   end
end
end
```

Part 5

```
function [n,s ] = CI_pathloss( rssi,Pt,G,d,fc )

%A and D are column vectors
%A (in dBm) represents PL
%d (in m)
% f is frequency in MHZ

D=10*log10(d);
N=length(D);
pl=-(rssi-(Pt+G)*ones(N,1));
 FSPL=20*log10((4*pi*fc*(10^6))/(3*10^8));
A=pl-FSPL*ones(N,1);
 n=A'*inv(D'*D)*D;
sum=0;
sum=(A-n*D)'*(A-n*D);
s=sqrt(sum/N);
new_pl=FSPL*ones(N+1,1)+n*[0;D];
figure(1);
semilogx(d,pl,'or')
end
```

Part 6

```
function [a,b,c] = FI_pathloss( rssi,pt,G,d )

pl=-(rssi-(pt+G));
B=pl;
D=10*log10(d);
N=length(D);
D_m_2=mean(D);
B_m_2=mean(B);
D_m=D_m_2*ones(N,1);
B_m=B_m_2*ones(N,1);

b=(D-D_m)'*inv((D-D_m)'*(D-D_m))*(B-B_m);
a=B_m_2-b*D_m_2;
k=B-a*ones(N,1)-b*D;
c=sqrt((k'*k)/N);
new_pl=a*ones(N+1,1)+b*[0;D];
 end
```

References

[1] A. Nag and S. C. Mukhopadhyay, "Smart Home: Recognition of activities of elderly for 24/7; Coverage issues," in *Proceedings of the 2014 International Conference on Sensing Technology, Liverpool, UK*, 2014, vol. 2, pp. 480-489.

[2] M. Li and H.-J. Lin, "Design and implementation of smart home control systems based on wireless sensor networks and power line communications," *IEEE Transactions on Industrial Electronics,* vol. 62, no. 7, pp. 4430-4442, 2015.

[3] R. S. Ransing and M. Rajput, "Smart home for elderly care, based on wireless sensor network," in *Nascent Technologies in the Engineering Field (ICNTE), 2015 International Conference on*, 2015, pp. 1-5: IEEE.

[4] E. Fernandes, J. Jung, and A. Prakash, "Security analysis of emerging smart home applications," in *Security and Privacy (SP), 2016 IEEE Symposium on*, 2016, pp. 636-654: IEEE.

[5] A. Anvari-Moghaddam, H. Monsef, and A. Rahimi-Kian, "Optimal smart home energy management considering energy saving and a comfortable lifestyle," *IEEE Transactions on Smart Grid,* vol. 6, no. 1, pp. 324-332, 2015.

[6] H. Ghayvat, S. Mukhopadhyay, X. Gui, and N. Suryadevara, "WSN-and IOT-based smart homes and their extension to smart buildings," *Sensors,* vol. 15, no. 5, pp. 10350-10379, 2015.

[7] F. L. Quilumba, W.-J. Lee, H. Huang, D. Y. Wang, and R. L. Szabados, "Using smart meter data to improve the accuracy of intraday load forecasting considering customer behavior similarities," *IEEE Transactions on Smart Grid,* vol. 6, no. 2, pp. 911-918, 2015.

[8] P. W. Schultz, M. Estrada, J. Schmitt, R. Sokoloski, and N. Silva-Send, "Using in-home displays to provide smart meter feedback about household electricity consumption: A randomized control trial comparing kilowatts, cost, and social norms," *Energy,* vol. 90, pp. 351-358, 2015.

[9] T. Qu, S. Lei, Z. Wang, D. Nie, X. Chen, and G. Q. Huang, "IoT-based real-time production logistics synchronization system under smart cloud manufacturing," *The International Journal of Advanced Manufacturing Technology,* vol. 84, no. 1-4, pp. 147-164, 2016.

[10] C. Prasse, A. Nettstraeter, and M. ten Hompel, "How IoT will change the design and operation of logistics systems," in *Internet of Things (IOT), 2014 International Conference on the*, 2014, pp. 55-60: IEEE.

[11] M. R. Palattella, N. Accettura, L. A. Grieco, G. Boggia, M. Dohler, and T. Engel, "On optimal scheduling in duty-cycled industrial IoT applications using IEEE802. 15.4 e TSCH," *IEEE Sensors Journal,* vol. 13, no. 10, pp. 3655-3666, 2013.

[12] D. J. Cook and S. K. Das, "How smart are our environments? An updated look at the state of the art," *Pervasive and mobile computing,* vol. 3, no. 2, pp. 53-73, 2007.

[13] C. M. Medaglia and A. Serbanati, "An overview of privacy and security issues in the internet of things," in *The Internet of Things*: Springer, 2010, pp. 389-395.

[14] Y. Liu and G. Zhou, "Key technologies and applications of internet of things," in *Intelligent Computation Technology and Automation (ICICTA), 2012 Fifth International Conference on*, 2012, pp. 197-200: IEEE.

[15] D. Miorandi, S. Sicari, F. De Pellegrini, and I. Chlamtac, "Internet of things: Vision, applications and research challenges," *Ad Hoc Networks,* vol. 10, no. 7, pp. 1497-1516, 2012.

[16] O. Vermesan and P. Friess, *Internet of things-from research and innovation to market deployment*. River Publishers Aalborg, 2014.

[17] M. Swan, "Connected car: quantified self becomes quantified car," *Journal of Sensor and Actuator Networks,* vol. 4, no. 1, pp. 2-29, 2015.

[18] R. Coppola and M. Morisio, "Connected car: technologies, issues, future trends," *ACM Computing Surveys (CSUR),* vol. 49, no. 3, p. 46, 2016.

[19] T. Bécsi, S. Aradi, and P. Gáspár, "Security issues and vulnerabilities in connected car systems," in *Models and Technologies for Intelligent Transportation Systems (MT-ITS), 2015 International Conference on*, 2015, pp. 477-482: IEEE.

[20] M. E. E. Alahi, X. Li, S. Mukhopadhyay, and L. Burkitt, "A Temperature Compensated Smart Nitrate-Sensor for Agricultural Industry," *IEEE Transactions on Industrial Electronics,* vol. 64, no. 9, pp. 7333-7341, 2017.

[21] Insight. (2017). *Is Tech the New Currency? Why You Need Modern IT*. Available: https://www.insight.com/en_US/learn/content/2017/05252017-is-tech-the-new-currency-why-you-need-modern-it.html

[22] H. Packard. (2016). *Low Power Wide Area (LPWA) networks play an important role in connecting a range of devices*. Available: https://h20195.www2.hpe.com/V2/getpdf.aspx/4AA6-5354ENW.pdf?ver=3.2

[23] (2017). *New research shows growing interest in industrial IoT adoption, companies in early stages*. Available: http://www.worldoil.com/news/2017/11/8/new-research-shows-growing-interest-in-industrial-iot-adoption-companies-in-early-stages

[24] M. Shirvanimoghaddam, M. Dohler, and S. J. Johnson, "Massive non-orthogonal multiple access for cellular IoT: Potentials and limitations," *IEEE Communications Magazine,* vol. 55, no. 9, pp. 55-61, 2017.

[25] T. 45.820. (August, 2015). *Cellular System Support for Ultra Low Complexity and Low Throughput Internet of Things*.

[26] A. D. Zayas and P. Merino, "The 3GPP NB-IoT system architecture for the Internet of Things," in *Communications Workshops (ICC Workshops), 2017 IEEE International Conference on*, 2017, pp. 277-282: IEEE.

[27] P. Kamalinejad, C. Mahapatra, Z. Sheng, S. Mirabbasi, V. C. Leung, and Y. L. Guan, "Wireless energy harvesting for the internet of things," *IEEE Communications Magazine,* vol. 53, no. 6, pp. 102-108, 2015.

[28] G. Anastasi, M. Conti, M. Di Francesco, and A. Passarella, "Energy conservation in wireless sensor networks: A survey," *Ad hoc networks,* vol. 7, no. 3, pp. 537-568, 2009.

[29] U. Raza, "From energy efficient to energy neutral wireless sensor networks," Ph. D. dissertation, University of Trento, 2015.
[30] N. C. Schoen, "Simultaneous multi-user audio re-transmission digital radio module," ed: Google Patents, 2003.
[31] M. Majima, S. Ujiie, E. Yagasaki, K. Koyama, and S. Inazawa, "Development of long life lithium ion battery for power storage," *Journal of Power Sources,* vol. 101, no. 1, pp. 53-59, 2001.
[32] G. T. 45.820. *Cellular System Support for Ultra Low Complexity and Low Throughput Internet of Things*. Available: https://portal.3gpp.org/desktopmodules/Specifications/SpecificationDetails.aspx?specificationId=2719
[33] P. Lescuyer and T. Lucidarme, *Evolved packet system (EPS): the LTE and SAE evolution of 3G UMTS*. John Wiley & Sons, 2008.
[34] NOKIA. (2017). *LTE evolution for IoT connectivity*. Available: https://resources.ext.nokia.com/asset/200178
[35] Cisco. *EC-GSM Support on the SGSN*. Available: https://www.cisco.com/c/en/us/td/docs/wireless/asr_5000/21-1/SGSN/21-1-SGSN-Admin/21-1-SGSN-Admin_chapter_01110.pdf
[36] B. Razavi, "A 900-MHz/1.8-GHz CMOS transmitter for dual-band applications," *IEEE Journal of Solid-State Circuits,* vol. 34, no. 5, pp. 573-579, 1999.
[37] Y.-P. E. Wang *et al.*, "A primer on 3gpp narrowband internet of things," *IEEE Communications Magazine,* vol. 55, no. 3, pp. 117-123, 2017.
[38] HUAWEI. (2017). *NB-IoT enabling new business opportunities.* Available: http://www.huawei.com/minisite/iot/img/nb_iot_whitepaper_en.pdf
[39] R. Ratasuk, B. Vejlgaard, N. Mangalvedhe, and A. Ghosh, "NB-IoT system for M2M communication," in *Wireless Communications and Networking Conference (WCNC), 2016 IEEE*, 2016, pp. 1-5: IEEE.
[40] C. S. Artin. (July 06, 2017). *NB-IoT, is the Darling of the GSMA, But Who Wins a Low Power High Stakes War?* Available: http://www.iotevolutionworld.com/iiot/articles/433141-nb-iot-the-darling-the-gsma-but-who.htm
[41] SIGFOX. (2017). Available: https://www.sigfox.com/
[42] T. M. W. 1.0. (2015). *Technical Overview of LoRa and LoRaWAN*. Available: https://www.tuv.com/media/corporate/products_1/electronic_components_and_lasers/TUeV_Rheinland_Overview_LoRa_and_LoRaWANtmp.pdf
[43] J. Petäjäjärvi, K. Mikhaylov, R. Yasmin, M. Hämäläinen, and J. Iinatti, "Evaluation of LoRa LPWAN technology for indoor remote health and wellbeing monitoring," *International Journal of Wireless Information Networks,* vol. 24, no. 2, pp. 153-165, 2017.
[44] L. Gregora, L. Vojtech, and M. Neruda, "Indoor signal propagation of LoRa technology," in *Mechatronics-Mechatronika (ME), 2016 17th International Conference on*, 2016, pp. 1-4: IEEE.
[45] A. Springer, W. Gugler, M. Huemer, L. Reindl, C. Ruppel, and R. Weigel, "Spread spectrum communications using chirp signals," in *EUROCOMM 2000. Information Systems for Enhanced Public Safety and Security. IEEE/AFCEA*, 2000, pp. 166-170: IEEE.
[46] M. Centenaro, L. Vangelista, A. Zanella, and M. Zorzi, "Long-range communications in unlicensed bands: The rising stars in the IoT and smart city scenarios," *IEEE Wireless Communications,* vol. 23, no. 5, pp. 60-67, 2016.

[47] E. Demirors, G. Sklivanitis, T. Melodia, S. N. Batalama, and D. A. Pados, "Software-defined underwater acoustic networks: toward a high-rate real-time reconfigurable modem," *IEEE Communications Magazine,* vol. 53, no. 11, pp. 64-71, 2015.
[48] Semtech, "SX1272/3/6/7/8: LoRa Modem Designer's Guide AN1200.22 " 2015.
[49] F. Adelantado, X. Vilajosana, P. Tuset-Peiro, B. Martinez, J. Melia-Segui, and T. Watteyne, "Understanding the limits of LoRaWAN," *IEEE Communications Magazine,* vol. 55, no. 9, pp. 34-40, 2017.
[50] J. Tiemann, F. Eckermann, and C. Wietfeld, "Multi-user interference and wireless clock synchronization in TDOA-based UWB localization," in *Indoor Positioning and Indoor Navigation (IPIN), 2016 International Conference on*, 2016, pp. 1-6: IEEE.
[51] P. San Cheong, J. Bergs, C. Hawinkel, and J. Famaey, "Comparison of LoRaWAN classes and their power consumption," in *Communications and Vehicular Technology (SCVT), 2017 IEEE Symposium on*, 2017, pp. 1-6: IEEE.
[52] Semtech. (2013). *SX1272/3/6/7/8: LoRa Modem Designer's Guide AN1200.13* Available: https://www.semtech.com/images/datasheet/LoraDesignGuide_STD.pdf
[53] Semtech, "LoRa SX1276/77/78/79 Datasheet, Rev. 4,", 2015.
[54] M. Shahajahan, "Analysis of propagation models for WiMAX at 3.5 GHz," ed, 2009.
[55] H. R. Anderson, *Fixed broadband wireless system design*. John Wiley & Sons, 2003.
[56] K. Hari, D. Baum, and P. Soma, "Channel models for fixed wireless applications," *IEEE 802.16 Broadband Wireless Access Working Group,* 2003.
[57] M. Hata, "Empirical formula for propagation loss in land mobile radio services," *IEEE transactions on Vehicular Technology,* vol. 29, no. 3, pp. 317-325, 1980.
[58] G. E. Athanasiadou, A. R. Nix, and J. P. McGeehan, "A microcellular ray-tracing propagation model and evaluation of its narrow-band and wide-band predictions," *IEEE Journal on Selected Areas in Communications,* vol. 18, no. 3, pp. 322-335, 2000.
[59] T. S. Rappaport, "Wireless Communications--Principles and Practice, (The Book End)," *Microwave Journal,* vol. 45, no. 12, pp. 128-129, 2002.
[60] P. E. Mogensen and J. Wigard, "COST 231: Digital mobile radio towards future generation system, final report," in *Section 5.2: on Antenna and Frequency Diversity in Gsm. Section 5.3: Capacity Study of Frequency Hopping Gsm Network*, 1999.
[61] S. Sun, G. R. MacCartney, and T. S. Rappaport, "Millimeter-wave distance-dependent large-scale propagation measurements and path loss models for outdoor and indoor 5G systems," in *Antennas and Propagation (EuCAP), 2016 10th European Conference on*, 2016, pp. 1-5: IEEE.
[62] Dragino. (2017). *LoRa Gateway*. Available: http://www.dragino.com/products/lora/item/119-lg01-s.html
[63] (2013). *Australian radiofrequency spectrum*. Available: https://www.acma.gov.au/-/media/Spectrum-Transformation-and-Government/Publication/pdf/spectrum_chart2013-pdf.pdf
[64] ThingSpeak. (2017). Available: https://thingspeak.com/
[65] Tektronix. (2017). *RSA306B Spectrum Analyzer*. Available: https://www.tek.com/sites/default/files/media/media/resources/RSA306B-USB-Real-Time-Spectrum-Analyzer-Datasheet-37W603750_0.pdf
[66] ATDI. *ICS telecom*. Available: http://www.atdi.com/ics-telecom/
[67] G. R. Maccartney, T. S. Rappaport, S. Sun, and S. Deng, "Indoor office wideband millimeter-wave propagation measurements and channel models at 28 and 73 GHz for ultra-dense 5G wireless networks," *IEEE Access,* vol. 3, pp. 2388-2424, 2015.